FILM GROWTH OF NOVEL FREQUENCY AGILE COMPLEX-OXIDE PIEZOELECTRIC MATERIAL

by

BINDU M.SREERAMAKAVACHAM
B.Tech., Jawaharlal Nehru Technological University, Hyderabad, India. 2001

A thesis submitted in partial fulfillment of the requirements
for the degree of Master of Science
in the Department of Mechanical, Materials and Aerospace Engineering
in the College of Engineering and Computer Science
at the University of Central Florida
Orlando, Florida

Summer Term
2007

ABSTRACT

Piezoelectric materials are well known for their applications in surface (SAW) and bulk acoustic wave (BAW) devices such as oscillators, resonators and sensors. Quartz has been the main material used in such applications. Ternary calcium gallium germanate (CGG) structure-type materials, so-called langasites, recently emerged as very promising because of their piezoelectric properties superior to quartz.

This thesis discusses the growth of langasite-type $La_3Ga_{5.5}Ta_{0.5}O_{14}$ (LGT) films by liquid phase epitaxy (LPE) technique and their chemical and structural characterization. In addition, the different techniques suitable for the growth of LGT are discussed and compared. To adjust the materials properties for given applications, doping by selected ions can be used. However, the dopants must be homogeneously distributed. In the current study, Al, Ti, Cr and Ca were investigated as dopants. In an earlier study, Al and Ti had been chosen because of their ability to substitute the octahedral site of LGT, normally occupied by Ga (CN=VI) with a segregation coefficient near unity in Czochralski growth. Doping with Ca and Cr has never been reported before, and therefore, the segregation behavior was unknown. In this study, Al, Ti and co-doping with Cr and Ca has been investigated for both X and Y-oriented films.

The dopant distribution in the films was quantitatively evaluated by Secondary Ion Mass Spectroscopy (SIMS), using ion-implanted LGT substrates as standards. The drop of dopant concentration, in the SIMS profile, allows for the identification of the film-substrate interface and to accurately measure the thickness of the films. The film thickness is found to be typically

of the order 0.5 to 2μm, depending on growth conditions. The solvent was found a reliable choice, as solvent ions were not incorporated in the films above the detection limits of the characterization techniques. A lead oxide solvent system is used as a solvent for the growth of LGT LPE films with different orientations. Extensive structural characterization was performed. The crystallinity of substrates and films grown with different orientations was compared by X-ray diffraction (XRD). The films show a very high structural perfection, with typically FWHM values of 0.035 for the (004) reflection of the XRD rocking curve. The films were also characterized by TEM. The optical transmittance of the films was characterized by Varian optical spectrophotometer, and the value obtained of approximately 80% is comparable with the transmittance value of the Czochralski grown polished substrate.

ACKNOWLEDGEMENTS

Dr. Christine F. Klemenz, my direct thesis supervisor, for her confidence when having chosen me to join her research group, for helping me to make my first steps into the research community; for encouraging me in innumerable ways. I am thankful for the wonderful experience I have had at the University of Central Florida. Thanks to my colleagues, Mr. Dhaval Shah and Ms. Zinki Monga, in the lab for their help and co-operation in fulfilling this work. I would like to thank Dr. Helge Heinrich and Mr. Mikhail Klimov for their help in doing the characterization of the films. Thanks to Ms. Karen Glidewell and Ms. Cindy Harle for ensuring that administrative work always ran smoothly. Thanks to my fellow graduate students for creating such an enjoyable study environment and for their willingness to devote time to helping out fellow students. I am very grateful to AMPAC and the director, Dr. Jim Pearson, for supporting me financially so that I could pursue this degree. Last, but not the least, my special thanks to Mrs. Jaya Balram, sweet little Sreeja and Ms. Madhulika for keeping me happy throughout the study.

This thesis is dedicated to my mother and my husband, who offered me love and encouragement throughout my life.

Finally, this thesis is dedicated to all those who believe in the richness of learning.

TABLE OF CONTENTS

LIST OF FIGURES

LIST OF TABLES

CHAPTER 1
INTRODUCTION TO LPE

In this chapter, a brief overview, principles and driving force of epitaxial growth is discussed. Some other important experimental parameters such as relative supersaturation, substrate misorientation and lattice mismatch, which govern the growth of thin films by LPE, are presented.

1.1 Fundamentals of LPE

Liquid Phase Epitaxy is a technique where a single crystalline layer is deposited from a solution on a particularly oriented single crystal substrate. Epitaxy originated from a Greek word 'επι ταξισ', which means "ordered on". LPE can be classified mainly into two types. One is 'homoepitaxy', in which the layer and substrate has same chemical composition and crystal structure and the 'heteroepitaxy', in which the layer and substrate have a different chemical composition but are similar in crystallographic relations. Under the growth conditions, both substrate and layer material must be chemically and thermally stable.

In 1963, at RCA laboratories, Nelson et al pioneered the application of LPE to the growth of the III-V compounds [1]. In fact, LPE has been the first technique used for the preparation of the epitaxial layers of compound semiconductors like GaAs, GaSb, InP, and ternary alloys. LPE has also been used extensively to grow the garnets for applications in magnetic bubble domain devices and optical isolators [2]. Experiments conducted in 1972 have proven that high quality

LPE layers can be grown on transparent optical materials, which has applications like waveguide lasers, amplifiers and saturable absorbers [3, 4].

The main advantages of LPE over vapor-phase epitaxy (VPE) techniques (molecular beam epitaxy (MBE), metal-organic chemical vapor deposition (MOCVD), or pulsed laser deposition (PLD)) are two fold:

a) High mobility of growth species at the substrate surface.
b) Higher concentration of growth species than in VPE.

In addition,

Using LPE, films with highest structural perfection containing low dislocation density and low concentration of point defects are possible. The growth is possible in the primary crystallization field (PCF growth) so there will not be any secondary phases present. The stoichiometry of the solution is controlled automatically. LPE grown films has better ordering as the dopant concentration is homogeneous. The films grown by LPE have transition to faceting and grow extremely flat surfaces. So the films require no polishing and they are free from mechanical damage or strain and are perfectly oriented. From 500 nm to several mm thick films can be grown by this technique, which can be used as substrates for the growth of multilayer structures by VPE. LPE is a non vacuum process, hence it is less expensive and simple apparatus can be used.

1.2 Phase equilibria

Reducing the solution temperature below the saturation temperature will act as the thermodynamic driving force for the LPE process. An example of a eutectic phase diagram used in the crystal growth from the high temperature solution is shown in figure 1. The solvent can be an element, a compound and a combination of compounds. The solute can be an element or a compound generally having a melting point higher than the solvent, but in theory, eutectic systems wherein solvent having higher melting point than solute can also be considered to grow crystals.

The solid curve represents the solubility line; the region above the curve represents the non saturated liquid solution, and the region below represents the saturated solution co-existing with the solute deposit.

When the ideal solution without chemical interactions is considered then, the solubility curve obeys the Arrhenius-type Van't Hoff equation

$$\ln\left(\frac{n_1}{n_2}\right) = -\frac{L_{sol}}{R}\left(\frac{1}{T_2} - \frac{1}{T_1}\right) \qquad (1.1)$$

where n_1, n_2 are the molar fractions of the solute in the saturated solution at temperatures T_2, T_1 respectively. L_{sol} indicates the heat of solution and R is the universal gas constant.

The spontaneous nucleation occurs when a solution of composition n_1 is cooled from temperature T_1 to T_2, in the absence of seeds and agitation. The solution in the region between

the liquidus line and the dashed line is undercooled or supersaturated. This region is called the metastable or Oswald-Miers region. A nucleus of a critical size must be formed before crystalline material is precipitated, which results in metastability.

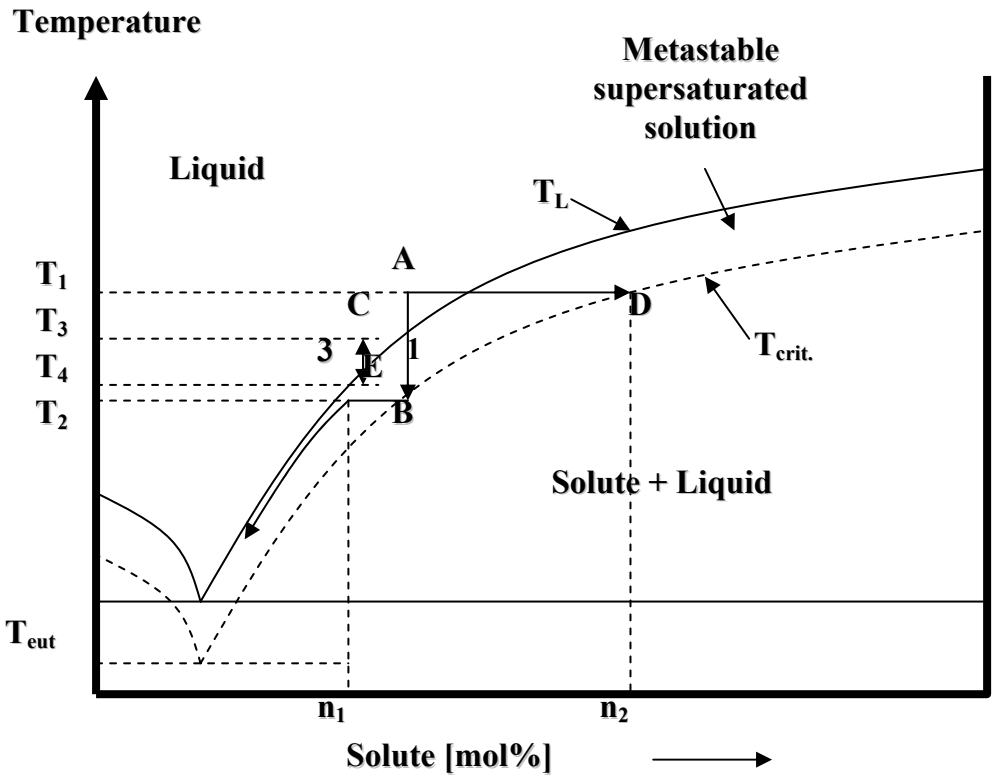

Figure 1 Typical solubility curve showing the path of the system composition during the process

The metastable Oswald –Miers (OM) region plays a vital role for the crystal grower because during the growth of large crystals the experimental conditions must be controlled to avoid unwanted nucleation. Occurrence of homogeneous nucleation is not possible in normal practical crystal growth conditions. It can only occur in highly supersaturated solutions. When there are no undissolved particles, the container walls or the surface of the solution will act as a source of heterogeneous nucleation.

Due to the presence of crystals which nucleate at B, crystal growth at lower supersaturation occurs along with the cooling of the temperature.

When the solvent is evaporated at a constant temperature, metastable region disappears and nucleation occurs at point D. On the other hand, the solvent is transported from saturated region (hot) to supersaturated region (cooler). In the Oswald-Miers region, the solution is supersaturated. The crucial condition to initiate bulk crystallization is to have a certain critical nucleus size r* where as in the OM region the spontaneous crystallization cannot start because of the existing atomic clusters which are smaller than r*. The nucleation mechanism and critical nucleus r* calculations will be discussed extensively in the coming sections. It is notable that in some eutectic systems, the Oswald-Miers region can be very large and when there are no nucleation sites, the respective supercooling of the solution can be as high as 200 K [5].

The solute excess can be deposited on to the substrate, and the substrate acts as a huge nucleation center when there is a situation in which the seed crystal is in contact with the supersaturated solution that still exists in the Oswald-Meirs region. Therefore, to achieve a slow and well controlled growth along the solubility curve, a very small supercooling below the saturation temperature T_1 is sufficient.

1.3 Theory of nucleation and epitaxy

The current section deals with the interface kinetics of the flat crystal surfaces. Figure 2 shows the idealized model of flat crystal surfaces. The general theory of nucleation (BCF theory) for atomically rough surfaces was proposed by Burton, Cabrera and Frank in the year 1951. 2D nucleation theory is convenient to treat a cylindrical nucleus of radius r and of height c corresponding to one growth unit (e.g. an atom or molecule).

The change in Gibbs free energy on formation of such nucleus is

$$\Delta G(r) = 2\pi r\gamma_e - \pi r^2 c\Delta G_v \tag{1.2}$$

where γ_e is the edge energy per unit length of the nucleus.

Free energy ΔG can be expressed in terms of the energy per growth unit (i.e., molecule) γ_m on the edge of the cylindrical nucleus. If the length of the molecule is 'a', then, $\gamma_m \approx a\,\gamma_e$ and so

$$\Delta G \cong \frac{2\pi r\gamma_m}{a} - \pi r^2 c\Delta G_v \tag{1.3}$$

and differentiation gives the radius of the critical nucleus as

$$r_s = \frac{\gamma_m}{ac\Delta G_v} \tag{1.4}$$

and the corresponding value of ΔG is

$$\Delta G^* = \frac{\pi\gamma_m^2}{a^2 c\Delta G_v} \tag{1.5}$$

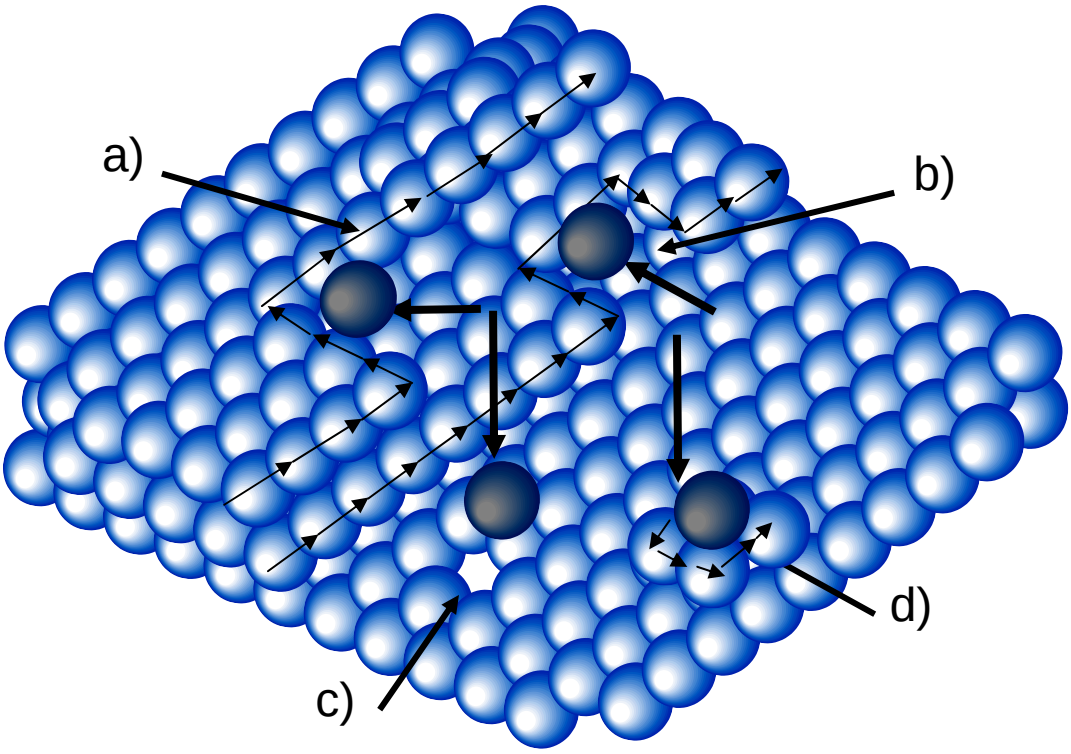

Figure 2 Idealized model of flat crystal surface a) step b) kink c) vacancy d) adatom

It is known that, free energy change per unit volume, $\Delta G_v = RT\sigma/V_M$, where V_M is the molar volume, σ is the relative supersaturation. Substituting the value of ΔG_v in the equation (1.5) gives

$$r_s^* = \frac{\gamma_m V_m}{acRT\sigma}$$

By substituting $V_M = N_A a^2 c$, where N_A is Avagadro's number, gives

$$r^* = \frac{\gamma_m a}{kT\sigma} \qquad (1.6)$$

And is approximately equal to

$$\gamma_m = \frac{L_{sol}}{6N_A} \tag{1.7}$$

where L_{sol} is the heat of solution.

Correspondingly,

$$\Delta G^* = \frac{\pi\gamma_m^2}{kT\sigma} \tag{1.8}$$

The number of molecules in a critical nucleus i* is expressed as

$$i^* = \frac{\pi r_s^{*2}}{a^2} = \left(\frac{\gamma_m}{kT\sigma}\right)^2 \tag{1.9}$$

Growth by 2D nucleation has a very high probability except at very low supersaturation values.

The three main parameters which can be controlled experimentally, compared to the other interdependent factors that govern the initial growth stages during LPE include supersaturation, substrate misorientation and lattice mismatch. These parameters are based on the following definitions and relations:

1.The relative supersaturation

The relative supersaturation measures the radius of the critical 2D nucleus in equation (1.2) is defined as

$$\sigma=(n-n_e)/n_e \tag{1.6}$$

where n and n_e are the actual and equilibrium concentrations of the solute at a given temperature T. This equation is used in this study to determine the supersaturation. Experimentally the real

equilibrium concentration n_e is difficult to measure. In the case of spiral growth, the relative supersaturation can be calculated from equation (1.5) by using mean values for the observed interstep distance and step height:

$$\sigma = \frac{19\gamma_m h}{y_o \varepsilon k T} = \frac{19 L_{sol} h}{6 y_o \varepsilon k T N_A} \tag{1.7}$$

For example, σ value for $YBa_2Cu_3O_{7-x}$ layers grown at 1273K from self-solvent $BaCuO_2$/CuO is 0.03 [40].

Apart from σ, undercooling can also be used to express supersaturation.

$$\Delta T = T_{sat} - T \approx \frac{\sigma R T^2}{L_{sol}} \tag{1.8}$$

where T_{sat} and T are the saturation and actual temperatures for the given solute concentration, respectively. At the growth temperature T=1173 K and the supercooling ΔT=10 K, the relative supersaturation σ = 0.041.

2.The substrate misorientation

The substrate misorientation is defined as the angular deviation of the substrate surface from a particular crystallographic plane. It requires the presence of open steps on the substrate surface .The interstep distance is related to the angle of misorientation φ, by

$$y_o = \frac{a_s}{\tan\varphi} \tag{1.9}$$

where a_s is the substrate lattice parameter.

The nucleation and development of the epitaxial layer is significantly affected by the presence of already existing steps on the surface of the substrate as shown in figure 3.

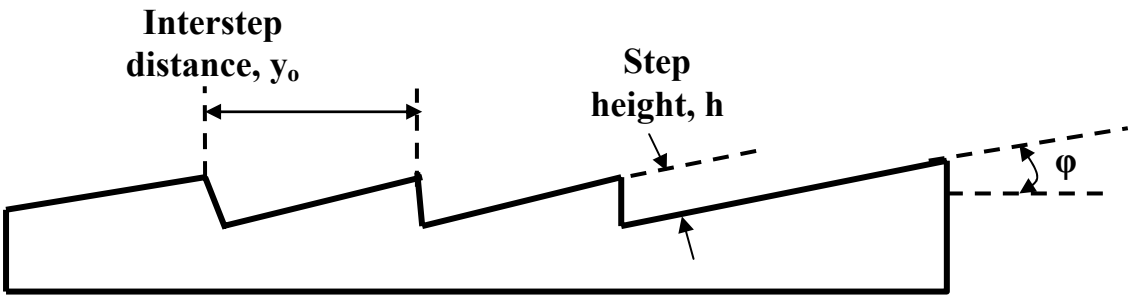

Figure 3 Misorientation of the substrate

Depending on the misorientation angle φ, four different growth mechanisms in the LPE of semiconductors were illustrated by Bauser [8]

a) $\varphi = 0^o$ – Facet growth.

In this case no initial steps were observed on the substrate surface. Also, a spiral growth with monomolecular steps is observed in the presence of screw dislocations. Therefore, a 2D nucleation is possible at higher supersaturations.

b) $0^o < \varphi \leq 0.1^o$ – Near-facet growth

In this condition, initial steps with large interstep distances were observed. Also, the layer surface is relatively smooth with the growth steps not exceeding the height of few unit cells.

c) $0.1^o < \varphi < 2^o$ – Terrace growth

In this case, several initial steps which bunch during the growth were seen. And, macrosteps (up to 100 to 200nm) with flat growth terraces results from step bunching (which increases the average height and distance of steps).

d) $\varphi \geq 2^o$ – Terrace-free growth

In this case, the layer surface has a wavy, sinusoidal structure as the misorientation is too high to form the flat growth terraces.

From the above discussion, it is evident that the desirable misorientation of LGT substrates is in the range of $0^o<\varphi<0.1^o$. This not only ensures a smooth layer surface but also provides sufficient number of initial steps to facilitate layer nucleation. The polishing of LGT crystals and their precise orientation determines the misorientation of available substrates.

A misorientation in substrates of typically $<0.5^o$, as seen in many cases, may lead to noticeable step bunching on the layer surface.

3. The substrate misfit

The substrate misfit is the difference between the crystallographic and thermal properties of the substrate and the epitaxial layer. The relative lattice mismatch at temperature T_1 can be expressed as

$$f_{latt,T_1} = \frac{(a_{S,T_1} - a_{L,T_1})}{a_{L,T_1}} \qquad (1.10)$$

where $a_{S,T1}$ and $a_{L,T1}$ are the lattice constants of the substrate and the layer at temperature T_1. In ideal homoepitaxy the lattice misfit is zero ($a_{S,T1}=a_{LT1}$). In heteroepitaxy, the lattice mismatch can either be tensile ($f_{latt,T1}>0$) or compressive ($f_{latt,T1}<0$).

1.4 Growth modes

Several parameters govern the subsequent development of the layer and the nucleation [9]. Some of the parameters are

- surface energies of the substrate, layer and their interface
- the solution supersaturation
- the lattice misfit between the substrate and the layer
- the substrate misorientation
- the surface diffusion at the growth temperatures
- the stoichiometry of the deposited compound
- the presence of impurities condensing inside the layer
- the partial pressure of reactive species etc.

The epitaxial growth modes can be classified into two main approaches.

The first approach is based on the surface tension at the layer-substrate interface. This includes the interfacial tensions of the atomic clusters on a flat substrate surface. There are three epitaxial growth modes were derived [10]. Depending on the decreasing wettability, they are:

1. The frank-van der Merwe (FVM) mode:

   In this mode, the complete wetting of the substrate and layer-by-layer growth takes place along with the macroscopic interstep distances [11].

2. The Volume-Weber (VW) mode:

   In this mode, a 3D island formation occurs due to the medium or low wetting [12].

3. The Stranski-Krastanov (SK) mode:

In this mode, first layer-by-layer growth takes place and continues with the formation of island. This mode is considered to be in between the FVM and VW modes. [13].

Composition of both layer and substrate play a vital role on the wettability of the substrate. A large lattice mismatch generally causes low wettability, as the lattice misfit and presence of impurities also affect wettability. The above said three growth modes considered to be fundamental growth modes. Different types of growth modes are shown in figure 4.

There are 4 other growth modes which consider the surface of the substrate has slight misorientation.

4. The screw-island growth:

   In this mode, hillocks and their coalescence grow due to the presence of screw dislocations.

5. The step-flow mode:

   In this mode, growth is achieved by using slightly misoriented substrates. This mode is similar to FVM mode.

6. The step-bunching:

   In this mode, several growth steps are bunched together in order to compensate a considerable substrate misorientation.

7. The columnar growth:

   This mode is the extension of the VW growth mode without coalescence of islands, due to the presence of anti-phase grain boundaries.

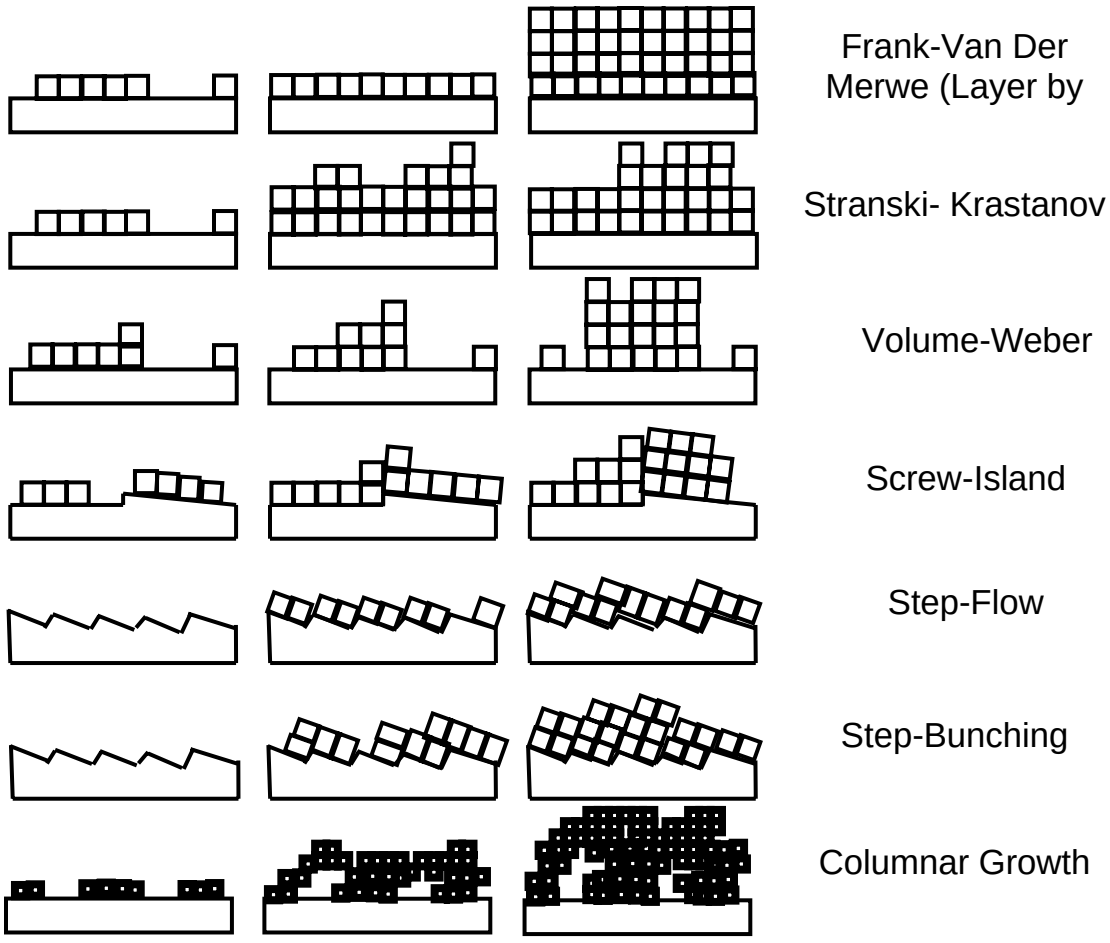

Figure 4 Different growth modes, according to [41]

To obtain a high quality LGT thin film layers, FVM is advantageous. Substrates with $\varphi = 0^{o}$ are required but this is possible only under the ideal natural face of LGT crystals. There are only few appropriate natural faces which suit among the bulk LGT crystal. In order not to waste the crystal material, many other oriented substrates are cut from it. There is possibility of a small substrate misorientation during the process of cutting and polishing, leading to the step-flow growth mode on the existing substrate steps. The step-flow mode is transformed into step bunching, if the substrate misorientation is in the order of 0.1^{o}. There are several factors that mislead the appearance of step-bunches even on slightly misoriented substrate. Some of the

factors which account for this are the variation in step source activity along the substrate surface, and the inhomogeneities in the solute supersaturation due to the incorporation of step-stopping impurities and liquid flow.

The appearance of step bunches could not be completely eliminated in the substrate and solution composition [14]. But can only be suppressed partially with the help of better oriented substrates, by lowering the supersaturation and controlling the flow of solution along the substrate surface. In optical applications, in order to avoid scattering losses the as-grown layer surface with step bunches (10-100nm in height) need to be polished. A severe problem of strong scattering losses which is induced from grain boundaries and coalescence of islands cannot be eliminated by polishing or any other treatment in VW or columnar growth mode.

1.5 Growth rate

When a crystal with a stepped interface comes in contact with a supersaturated solution, the growth occurs in following steps [43]:

1. Transport of solute to the neighborhood of crystal surface.
2. Diffusion through a boundary layer, adjacent to the surface, in which a gradient in the solute concentration exists because of depletion of material at the crystal-solution interface.
3. Adsorption on the crystal surface.
4. Diffusion over the surface.
5. Attachment to a step.
6. Diffusion along the step.

7. Integration into the crystal at a kink.

The transportation process by which the solute is transferred to the crystal is crucial to the growth of good quality crystals and can be divided into two stages.

a) Solute moves to the nearest substrate due to the natural or forced convection.

b) Solute particles diffuse to the substrate surface via the diffusion boundary layer.

The difference in the concentration of the solute acts as the driving force to diffuse through the boundary layer. When the kinetic process is rapid compared to the volume diffusion, the solute concentrate at the interface will be approximately equal to the equilibrium value. But in the case of bulk solution, the solute concentration is higher and almost constant. According to Nernst, the solute concentration gradient is considered to be uniform over the boundary layer width. The linear growth rate is given by,

$$\upsilon = \frac{D}{\rho}\frac{(n - n_e)}{\delta} \qquad (1.11)$$

where n and n_e are the solution and equilibrium solute concentrations, D is the diffusion coefficient, ρ is the crystal density, and δ is the width of the diffusion boundary layer.

This equation (1.11) is used in this study to calculate the growth rate of the films.

In 1958, Carlson assumed the laminar flow of the solution over a face of the crystal. He derived an expression for the rate of growth of the crystal, which results in the solute diffusion boundary-layer width, and is given by

$$\delta = \left\{ 0.463 \left[\frac{\eta}{\rho_{sn} D} \right]^{1/3} \left[\frac{u \rho_{sn}}{\eta L} \right]^{1/2} \right\}^{-1} \tag{1.12}$$

Where ρ_{sn} is the solution density, η is the dynamic viscosity of the solution, U is the flow velocity, and L is the length of the substrate face.

When a crystal is rotated in the solution, a similar variation in the growth rate was observed by Burton, Prim and Slichter in 1953. The boundary-layer thickness expression given by them is,

$$\delta \approx 2^{2/3} D^{1/3} \left[\frac{\eta}{\rho_{sn}} \right]^{1/6} \omega^{-1/2} \tag{1.13}$$

where ω is the angular velocity of the crystal rotation. The thickness δ varies as $\omega^{-1/2}$, and usually, it is approximately 500-750 nm for rotation rates of 30-50 rpm. For instance, if the diluted solution of LGT in the PbO solvent has $\eta = 4.25 \times 10^{-2} gcm^{-1}s^{-1}$, $\rho_{sn} = 4.964 gcm^{-3}$, and $D \approx 3 \times 10^{-5}$ cm^2s^{-1}, the diffusion layer thickness $\delta = 5 \times 10^{-5} cm$ for the rotation rate $\omega = 0.5 s^{-1}$ (30 rpm).

At the substrate edges, the solute flow is comparatively fast, which leads to the faster growth of edges than the central parts. This causes the hooper growth or inclusion of the mother solution. To eliminate this problem, D. Elwell and H. J. Scheel developed an expression for the maximum size of the inclusion-free crystals by taking the hydrodynamics into account, from the equation derived by Carlson [24]. The equation for the maximum stable linear growth rate is given as

$$\upsilon_{\max} = \left(\frac{0.214 D u \sigma^2 n_e^2}{Sc^{1/3} \rho_{sn}{}^2 L} \right)^{1/2} \tag{1.14}$$

Here $Sc = \eta/\rho D$, which is known as Schmidt number, a dimensionless constant for a liquid at a particular temperature.

As it is known $u = \pi L\omega$, the above equation can be rewritten into

$$\upsilon_{\max} = \left(\frac{0.214\pi D\omega\sigma^2 n_e^2}{Sc^{1/3}\rho_{sn}^{\ 2}} \right)^{1/2} \tag{1.15}$$

Table 1 Parameters for the calculation of maximum stable growth rate υ_{max}.

Parameters (units)	Symbol	$PbO\text{-}MoO_3$ Solvent
Temperature (^oC)	T	900
Solution mass(g)	m_{sn}	109.1
Solution volume (cm^3)	V	22.0
Solute mass (g)	m_s	8.0
Initial solute concentration (g cm^{-3})	N	0.364
Supersaturation	Σ	~ 0.04
Equilibrium solute concentration (g cm^{-3})	n_e	$n_e=n/(\sigma+1)$
Solution density (g cm^{-3})	ρ_{sn}	4.96
Solution viscosity ($gcm^{-1}s^{-1}$)	H	$4.25x10^{-2}$ [24]
Diffusion coefficient ($cm^2\ s^{-1}$)	D	$3x10^{-5}$ [23]
Angular rotation velocity (s^{-1})	Ω	0.5
Boltzmann constant (JK^{-1})	K	$1.38x10^{-23}$
Schmidt number	Sc	285

This equation (1.15) is used in this study to evaluate the maximum stable growth rate of the films and can be defined as the growth rate below which the incorporation of inclusion can be

prevented. The experimental values of the parameters required to calculate the maximum stable growth rate is given in table 1.

1.6 Other LPE techniques

From the solubility diagram (figure 1), it is evident that every LPE process consists of five successive steps:

- heating the solution above the saturation temperature
- liquid homogenization
- supersaturating the solution via cooling
- substrate introduction
- Finally, removal of the substrate from the solution after a growth time t.

The temperature vs. time profile that applied during the LPE growth is shown in figure 5 [43].

The system is heated up to the temperature T_{hom} and is equilibrated. The temperature T_{hom} is above the saturation temperature T_s. To attain the supersaturated solution, the system is then cooled under T_s. Different cooling techniques that can be used are

a. Slow cooling: In this method, substrate is brought in contact with the saturated solution which is at the saturation temperature T_s. After attaining the temperature T_{end}, by linear cooling of the system, the substrate is taken out from the solution with the grown layer.
b. Step cooling or isothermal growth: In this method, the solution is cooled to T_{iso}, after its homogenization. T_{iso} is lower than T_s, but is not enough for spontaneous precipitation. Epitaxy starts from the supersaturated solution kept at T_{iso}.

c. Supercooling: The substrate is dipped in the supersaturated solution at temperature T_{iso}. The growth takes place during the continuous cooling of the system up to T_{end}.

d. Solid-liquid coexisting solution: In this method, the cooling procedure is the same as supercooling, but the solution temperature is decreased below T_s, which allows spontaneous precipitation to be initiated before dipping the substrate.

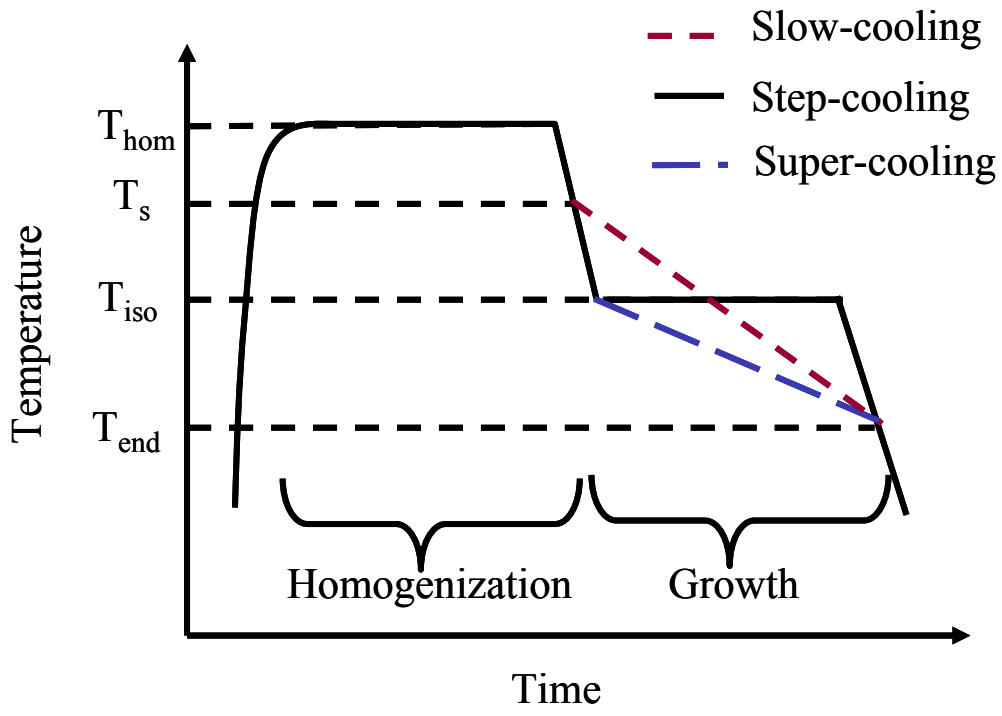

Figure 5 Temperature vs. time profile during LPE

The equilibrium cooling enables the film growth to start at the saturated solution, which results in a very low degree of supersaturation. Hence, the accurate determination of saturation temperature T_s is important for each solute concentration.

However, exact information about T_s is not required for both step-cooling and supercooling processes. In addition to this, the driving force for nucleation is provided by the initial

supercooling, which occurs more uniformly over the substrate and results in the growth of much smoother layers [21]. Solid solution from the solid-liquid coexisting solution grows with the expense of solids grown on the heterogeneous sites such as walls of the crucible. For this reason, the solution always remains saturated with solute and provides near equilibrium supersaturation during cooling. However, solid deposition on crucible walls does not contribute to the expected growth of solid layer on the substrate material. This solid deposition varies depending on the size, shape and location of the already existing precipitates within the crucible.

Based on the geometry of the arrangement, LPE techniques are categorized into:

1. *Tipping.* A boat shaped crucible containing both substrate and saturated liquid solution at its opposite ends, is tilted so that the solution lies towards the lower end. Once the growth temperature is attained, the crucible is tipped to allow the solution to flow over and immerse the substrate. This growth process continues until the crucible is tipped to its original position.

2. *Sliding boat.* A machined graphite holder, containing the substrate slides to contact saturated solutions contained in numerous wells.

3. *Dipping.* A preheated substrate, held either in a vertical or horizontal plane, is dipped in the solution for the particular amount of growth time.

Among above mentioned techniques, the tipping and sliding boat techniques are of great use for LPE growth of semiconductors, where multilayer semiconductor structures should be grown in the atmosphere control. The dipping technique was applied for LPE of various oxide layers [22]. This technique is simple and quick when comparing with the other two techniques. The main

feature here is the substrate is directly dipped into the supersaturated solution. The crucible that is heated by means of electric-resistance heating contains this solution. For these reasons, in this work, the dipping technique is used for the growth by LPE of LGT thin layers

CHAPTER 2
LANGASITE MATERIALS

Langasite type materials including $La_3Ga_5SiO_{14}$ (LGS), $La_3Ga_{5.5}Ta_{0.5}O_{14}$ (LGT) and $La_3Ga_{5.5}Nb_{0.5}O_{14}$ (LGN) have the structure of Ternary calcium gallium germinate, $Ca_3Ga_2Ge_4O_{14}$ (CGG) structure-type, are discovered in 1980 [15]. LGT belongs to the space group P321, similar to but not quite the same as quartz ($P3_121$, or $P3_221$). Main differences between the quartz and CGG type materials are the absence of a screw axis and lack of handness symmetry.

2.1 Crystal structure

LGT belongs to trigonal system and is a uniaxial crystal. According to H. Takeda, each unit cell contains two formula units and the lattice constants are a=8.228 Å and c=5.124Å [20]. The schematic of LGT structure is shown in figure 6. A unit cell consists of six lanthanum atoms, eight gallium atoms, two tantalum atoms and twenty eight oxygen atoms. The La^{3+} ions are positioned in the polyhedral sites surrounded by eight oxygen atoms. The shape of the polyhedron is as a distorted Thomson cube, as the interatomic distance La and O varies from 2.354Å to 2.854 Å. Ga1 octahedral site is occupied by Ga and Ta atoms and the occupancy ratio is 0.54:0.46 [16]. Ga atoms will occupy the Ga2 and Ga3 tetrahedral sites. The average interatomic distance between Ga2 and O is 1.83 Å and that between Ga3 and O is 1.85 Å.

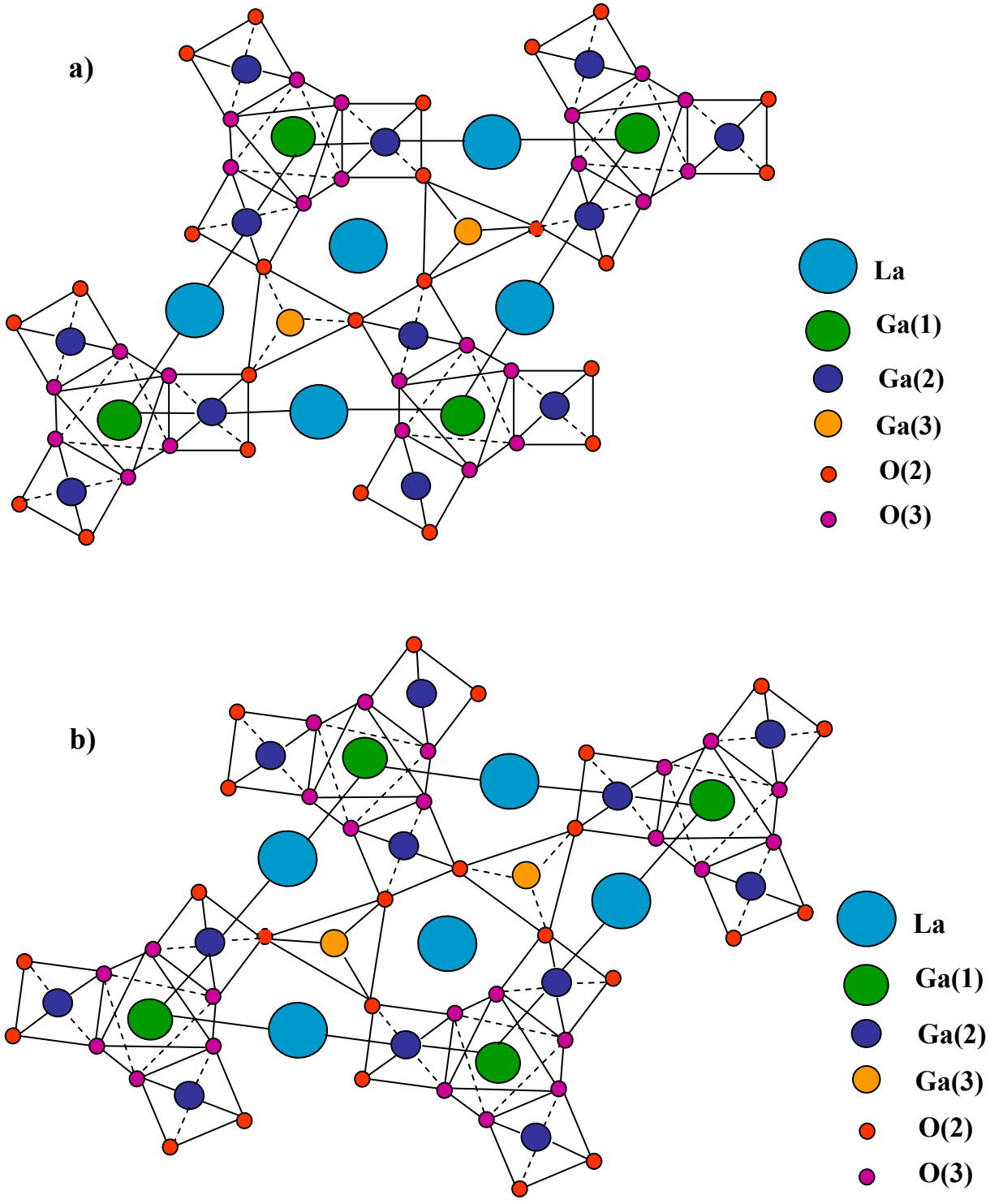

Figure 6 Arrangement of coordination polyhedra in the $La_3Ga_{5.5}Ta_{0.5}O_{14}$ crystals structure.

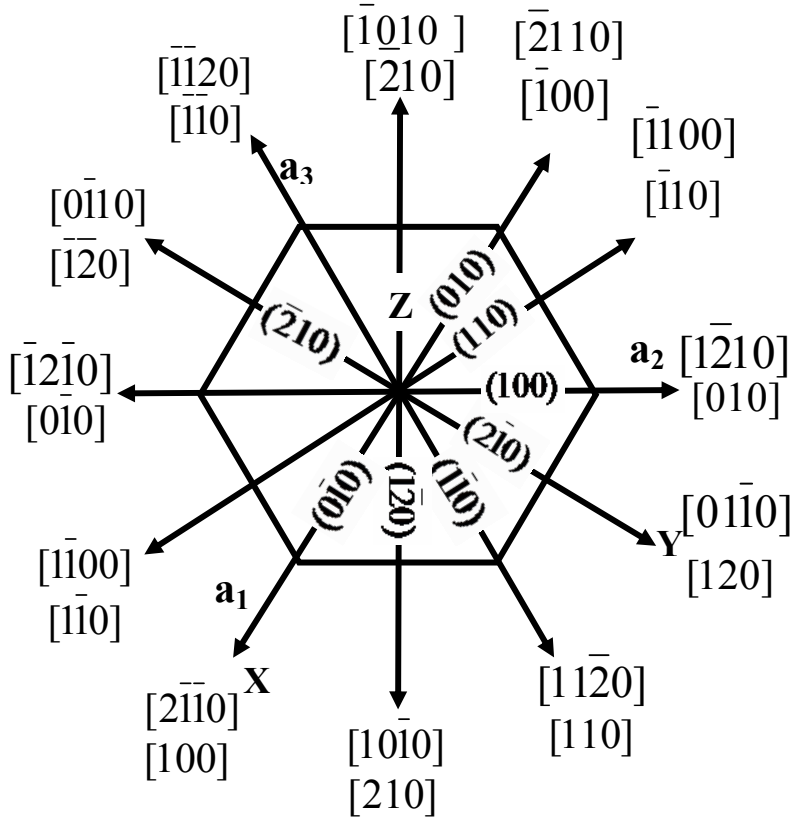

Figure 7 Schematic of crystal physical axes X, Y, Z and conventions used in trigonal-hexagonal system

In general, crystal physical axes are important to evaluate the material for certain applications. Though this study is not intended to discuss any applications, the crystal physical coordinate system is mentioned for the sake of better understanding. As shown in the above figure, X, Y and Z are the crystal-physical axes.

Indices of the planes are given by (hkl) = (hk.l)

$$(hkil) = (h\ k - (h+k)\ l)$$

Indices of the directions are given by [uvw] = [uv.w] = [u*-t* v*-t* 0 w*]

$$[u^*v^*t^*w^*] = [2u-v\ 2v-u\ -(u+v)\ w]$$

The terms X, Y and Z oriented substrates refer to the surfaces normal to the crystallographic axes X, Y and Z directions, with YZ, XZ and XY in-plane axis respectively [26].

2.2 Advantages of ternary Langasites over Quartz

Langasites (LGX, with X=S, N, T) are novel piezoelectric materials investigated for their acoustic and electromechanical properties. Both LGX and quartz have the same point group (32) symmetry. Also, both can be used for making temperature-stable BAW and SAW devices, because of their unique ability to have temperature-independent crystal orientations. LGX is better than quartz with respect to electromechanical coupling strength. The slower acoustic velocity of LGX compared to quartz materials enables LGX to find a wide range of applications in miniaturized wideband SAW filters. These are used in portable wireless devices. It has been postulated that LGX has higher acoustic loss than quartz owing to its disordered structure. However, there is not consensus among the scientific community on the origin of the losses observed in LGX, as it can also be due to the presence of crystal defects.

All ternary langasites have the same crystal structure with quite similar properties. However, there exist differences in the properties of these compounds, such as: lattice parameter, thermal expansion coefficient, dielectric constant, acoustic velocity and electromechanical coupling constant, mainly due to variation in their compositions. These slight differences can significantly affect the device properties. On the other hand, composition does not play a great role for the differences in properties of quartz family compounds. Differences are also associated with their physical appearances due to external action of temperature and radiation, for example.

The LGX structure is highly complex, that is mainly due to the distinct occupation of the cations as A, B, C and D sites. They are classified as three dodecahedral (Site A), one octahedral (Site B), three large tetrahedral (Site C) and two small tetrahedral (Site D) sites. The size and electron charge of each of these sites is limited and is characteristic of individual sites. However, this limitation does not greatly influence reduction of disorderness of the LGX materials. Several polymorphs of quartz also have highly complex crystal structures with the variation of ions within the rhombohedral crystal structure.

Materials with a perfectly ordered structure have great crystal performance (Q) due to the well established structure factor. However, high quality single crystal of Y-cut Langasite isomorphs LGN and LGT have higher material Q than quartz. The maximum published Q value of LGN (BAW) is 2.2×10^{13} Hz, and for LGT (BAW) it is 2.9×10^{13} Hz [27]. Hence, the disorder of the structure does not seem to be of great influence in these particular cases.

Presence of Ga_2O_3 in LGX group compounds raises the cost of these materials and makes quartz the economical substitute of these compounds. However, the better performance of LGX compounds in BAW and SAW devices makes them most suitable for devices where a highest-performance in desired. Then, they surpass quartz. LGX compounds can show strong facet development in crystal external morphology. Faceting in Czochralski-grown LGX depends on different factors, such as pull orientation, chemistry, and growth conditions. It has been observed that LGS grows round with no facet development, whereas LGT and LGN can show faceting or not. Development of facets is a common property of quartz crystals.

Table 2 Comparison of Quartz with other Langasite type materials.

Material	K^2 (%)	SAW Velocity (m/s)	ε_{11}	ε_{33}
Quartz	0.134	3156	4.53	4.68
LGS	0.3-0.38	2350	19.62	49.41
LGN	0.43	2300	20.089	79.335
LGT	0.38	2220	18.271	78.95
CTGS	0.322	2774	16.7	21.5
CNGS	0.266	2905	18.67	29.97

Ordered langasites compounds (CTGS and CNGS) can be the powerful substitutes of quartz due to the properties such as low acoustic loss, high quality factor for acoustic wave resonator applications, high electromechanical coupling factor and reduced incoherent phonon scattering. In addition, the presence of heavy elements in these materials can also contribute in reducing the phonon energy of these crystals.

2.3 Comparison of LPE and Czochralski growth of LGT

The two growth methods Liquid phase epitaxy (LPE) and Czochralski (CZ) are fundamentally different. LPE and/or solution growth technique use a solution with different composition from that of the crystal or film whereas CZ method uses the melt of same composition to that of the crystal. LPE is a near thermodynamic equilibrium method to grow single crystalline thin films from a solution on various substrate materials. Due to the small thermal and chemical gradients

that drive the process, this method is highly sensitive to substrate surface defects and process parameters.

In LPE, wafers of the bulk crystals grown by CZ method are used as substrates to grow thin films. The relative variation in the amounts of solvent and solute required for the LPE growth technique can be considered with the help of a phase diagram. However, CZ does not require great information from phase diagrams as the compound composition and solubility are less variable. Only knowledge of congruency is required for CZ growth. In LPE, after the required level of the film is grown, the parent solution along with a residual amount of solute will not be used for any further consideration in the LPE process. On the other hand, in the case of CZ, the residual melt after the crystal growth can be reused with little or no modification of the composition. The size of the crystals in CZ technique can be controlled as per the requirements. For a same material, the size of a crystal that can be grown from a solution is typically less than from CZ growth. LPE growth can be achieved at low temperatures, such as 900°C for LGT films, as the low-melting solvent ensures reduction in overall growth temperature. In contrast, the temperature that is applied in CZ for the growth of LGT is around 1470^{o}C, which is much higher than that of LPE growth. The precise temperature control, however, is very important in both the methods.

For LGT, experimental setups used for both these techniques use vertical furnaces, with RF-heating for CZ and resistance heating used for LPE techniques. The weighing mechanism of the crystal plays an important role in controlling the overall growth process in CZ technique. On the

other hand, for LPE, the weight control mechanism is not of much importance, as the total weight change of substrate due to the film growth is very less.

For LPE, substrate and process parameters such as supersaturation, substrate rotation, hydrodynamics are the determining factors for the quality of the film. In CZ, the seed quality and operating parameters (rotation, weight, temperature and other factors) are important.

The crystal homogeneity and perfection required for device fabrication are often compromised due to material defects and inconsistent operational parameter related problems in the CZ process. Reliable parameters and reproducibility remain challenges in this process. Growth instability and constitutional supercooling of the melt are often observed in the case of high viscosity of the melt. No wafers or films can be directly obtained from CZ technique, in other words, machining of the bulk crystals is necessary for device manufacture.

If all substrate and growth conditions are sufficiently well adjusted, reproducibility can be achieved in LPE growth. Also, in this case, very flat surfaces can be obtained which do not require further machining. Such surfaces can be directly used for device manufacture.

CHAPTER 3
FILM GROWTH

3.1 Growth systems

Two different LPE growth systems are used in this study. For preliminary experiments, a growth system with a single zone furnace and Honeywell temperature controller is used, shown in figure 8. Once the growth conditions are established, a much sophisticated growth system, Pt coil wound three zone furnace having Eurotherm temperature controller is set up.

Figure 8 Single zone LPE growth system.

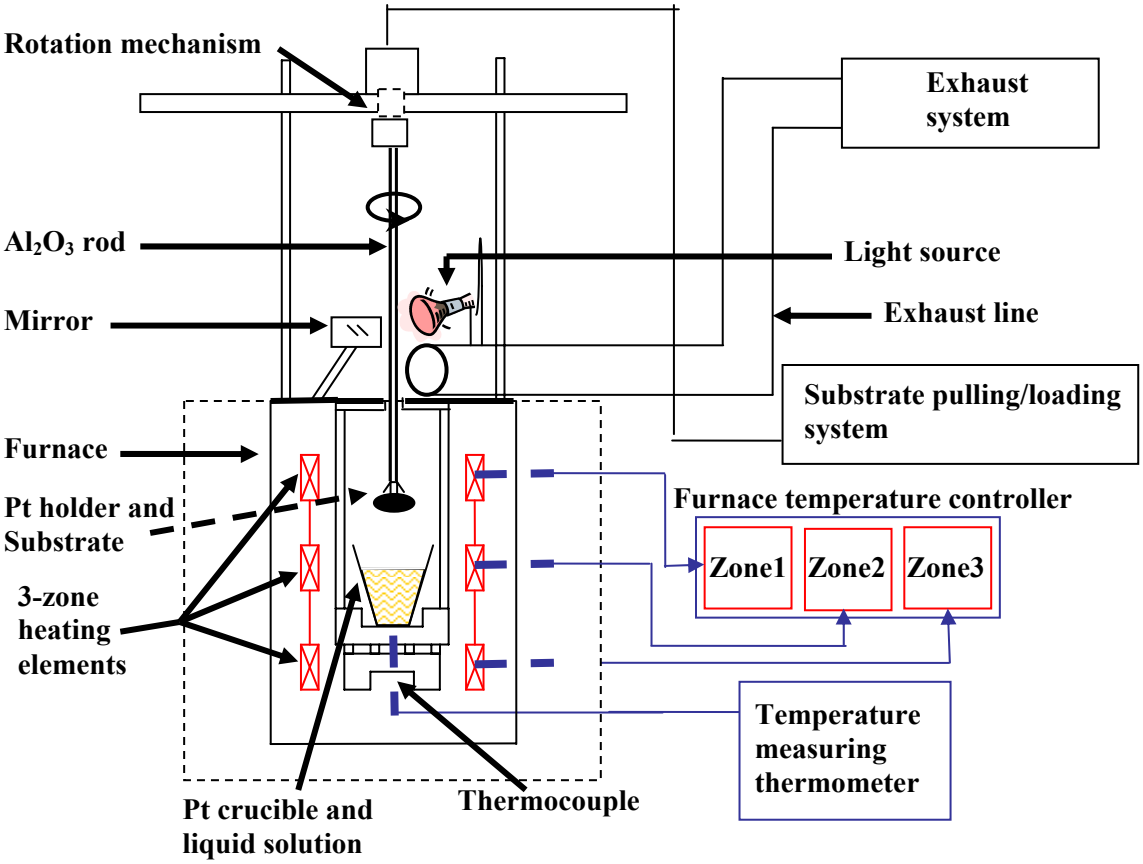

Figure 9 Schematic of the LPE growth system

A schematic and the picture of the three zone furnace are shown in figures 9 and 10, respectively. Both the systems have vertical furnaces, containing Al_2O_3 refractory lining inside them. Pt-crucible containing supersaturated solution is kept inside the furnace as shown in the figure. At the top of the furnace, a rotation mechanism that is capable of rotating up to 250 rpm is provided for Al_2O_3 holder rod.

The end of this rod carries a Pt-holder to hold substrate that needs to be dipped and rotated during the LPE growth process. The pulling mechanism takes care of withdrawal of the holder along with the substrate after the film formation.

A mirror is used to observe and inspect the substrate dipping, rotation, interface establishment between substrate and solution and any formation of crystallites on the surface of the solution that needs to be taken out for smooth process.

Figure 10 Picture of 3 zone Pt furnace LPE growth system

The furnace heating uses electrical induction by means of an induction coil that surrounds the Al_2O_3 chamber. A thermocouple at the bottom of the crucible allows close reading of temperature values associated with the solution.

The fumes generated during the process are carefully suctioned from the central exhaust system provided on the top of the furnace.

As already mentioned, this is a single zone furnace mainly designed for the preliminary LPE growth experiments. However, a three zone furnace is quite recommended as it is more capable of controlling near thermodynamically equilibrium temperatures than a single zone furnace.

3.2 Selection of solvent

To find a suitable solvent for a given crystal system is one of the most significant and complicated task. The former concept that is followed for this is 'Simila similibus solventur' which means similar is dissolved in similar. The optimal choice of solvent should have similarities in the type of bonding of the solute. At the same time, it should possess sufficient crystal-chemical differences. This prevents the solvent species incorporation into the solute structure (i.e. excessive solid solubility). For example, metallic solutions are used for the growth of metals, and oxide or fluorides or a mixture of both can be used for high-melting oxide compounds

3.2.1 Properties of ideal solvent

. Ideally solvent with same ions and cations as that of a crystal is preferred. Otherwise, then the following properties should be possessed by the solvent.

- High solubility for the crystal constituents.
- The crystal phase should be the only stable solid phase.

- Differences of valances between solute and solvent ions (no elements which may be incorporated into the crystal) and/or large differences of ionic radii.
- Appreciable change of solubility with temperature
- Viscosity in the range of 1-10cp.
- Low melting point.
- Low volatility (except for solvent evaporation technique).
- Appropriate density.
- Easy to separate from the crystal by chemical or physical means.
- Low toxicity.
- Availability at high purity and low cost.

Generally, there is no solvent which fulfills all these ideal properties, and a compromise is necessary.

3.2.2 Solvent search for Langasites

The majority of solvents used in the growth of oxides can be broadly categorized into: Pb and Bi containing compounds (PbO, PbO–PbF_2, Bi_2O_3,…); borates (B_2O_3, $Na_2B_4O_7$, BaB_2O_4,…); vandates (V_2O_5, $NaVO_3$,…); molybdates and tungstates (Na_2MoO_4, $K_2W_2O_7$,…); halides (LiCl, NaCl, KCl, $BaCl_2$,…); sulphates, phosphates, hydroxides and others (Na_2SO_4, $Zn_3(PO_4)_2$, KOH,…).

Alkali vandates, molybdates and tungstates are commonly used for flux growth of complex oxides such as silicates and germanates. Austerman [28] used Li_2MoO_3– MoO_3 flux for the growth of BeO films. He observed that the crystal habit was influenced by impurities, and

changed in shapes from pyramids, prisms, to platelets with reducing MoO_3 content in the solution. In the case of LGT, $Li2MoO_4$:MoO_3 fluxes with ratios ranging from 1:1 to 1:4 were attempted for flux growth, top seeded solution growth (TSSG), and LPE experiments of LGT and LGS, within the temperature range of 1150–850^oC [29]. The langasite phase did not crystallize in the investigated region, in the lower temperature range, La, $Li(MoO_4)_2$ grow epitaxially on the substrates [29]. Strong interface reactions took place, even for solute concentrations up to 50 wt%. Bi_2O_3-based fluxes have some similarities with PbO fluxes, and can lead to lowering of the liquidus temperature when added to $BaO–B_2O_3$ fluxes. However, the presence of large rare-earth (RE) ions can cause substitutions. In LGS systems, Bi^{3+} with radii of $r^{VIII}{}_{Bi}{}^{3+}$=1.17 Å would easily substitute La^{3+} with $r^{VIII}{}_{Bi}{}^{3+}$=1.16 Å (ionic radii taken from Ref. [30]). $PbO–B_2O_3$ fluxes as well as $BaO–BaF_2–B_2O_3$ ternary solvent systems were successfully employed in LPE of garnets for magnetic bubble applications [31, 32]. PbO-based fluxes were also employed for the growth of perovskites ABO_3 (A=La, Nd, Pr; B=Ga) [33]. The advantage of borate-containing fluxes is lower volatility, but this can be attained at the expense of a higher viscosity. B_2O_3 is commonly used as an additive (about 1–2%). PbF_2 and PbO_2 are also generally used as additives, in order to reduce the nucleation and to preserve the life of the Pt crucibles, respectively. Preliminary LGS flux experiments were carried out using PbO with different additives [29]. The addition of B_2O_3 and/or PbF_2 leads to the crystallization of $LaBO_3$ and LaF_3, respectively, and these additives were therefore avoided in further studies.

Whereas early studies yielded only LGO, LGSLPE films could be successfully grown from PbO fluxes containing 15–20 wt% stoichiometric LGS and 1% PbO_2 [29]. However, due to the

stability field of LGO, the LGS film growth temperature had to be set very close to the melting temperature of PbO, which resulted in a highly viscous solution, and crystallization of LGO as competing secondary phase. Hence, MoO_3 was used as an additive [34], as it forms a binary eutectic with PbO thereby allowing lower growth temperatures and lower viscosity of the growth solution. Several possible reasons were postulated for the fact that the LGS phase could not be obtained from the same flux, e.g. without LGS substrate. First, LGO is the stable phase in the higher temperature range. Once formed, LGO continues to grow and prevents the formation of the LGS phase while cooling down. It is also known that crystals from other phases may grow in the stability field of another material, mainly when a seed (or substrate) of the required phase is present. For this reason, when the LGS substrate is present, epitaxial growth of LGS is energetically favored, which is in agreement with earlier observations on the growth of metastable phases [2, 35].

Based on the above discussed literature, for the current work, a PbO: MoO3 solvent system with 10:1 ratio was used. Due to the toxicity of PbO, this solvent should be avoided whenever possible. However, as discussed previously, other solvent systems didn't allow obtaining high-quality LGX films.

In-situ doping is performed by mixing the additive directly to the starting chemicals, as explained further below in the experimental section. LGT films with Ti and Al co-dopants were successfully demonstrated in an earlier study [36]. However, nothing was known on other dopants, like Cr and Ca, investigated in this study. Especially co-doping by more than one ion

can significantly change the morphology of the films, as it modifies the properties of the solution as well.

3.3 Substrate preparation

The quality of the LPE grown film depends mainly on the substrate surface imperfections and strains developed due to crystal defects. Thus, surface preparation of the substrate should be given much consideration in LPE. This surface preparation includes grinding, polishing and chemical etching. Annealing is one other proven method for efficiently producing the surface steps [37]. Chemical etching is the final step for removal of the damaged surface layer of polished substrates [38, 39].

As langasites are similar to garnets and perovskites families, the most suitable etchant is ortho-phosphoric acid (H_3PO_4). Best etching was obtained with H_3PO_4 at 130^oC with the duration ranging from several minutes to hours (2-3hrs) [44]. This also allows revealing striations and other crystal defects. Properly adjusted etch conditions and the use of forced convection result in a smooth substrate surface after the etching [29, 34]. In langasite type crystals, the two sides of Y- and Z- oriented substrates have the same termination. In contrast, the two X- cut substrate surfaces are not equivalent. They behave differently upon etching due to the polarity of the X-axis.

3.4 Growth procedure

The Pt-crucible containing solution is covered with a Pt-lid to prevent PbO evaporation when it is subjected to high temperatures during heating and soaking. It is kept in the furnace where the

desired temperature gradient is available for the process of LPE. The furnace is initially heated at a rate of 50^{o}C/hour up to the temperature of 800^{o}C, and later the heating rate is reduced to 20^{o}C/hour to attain up to 920^{o}C temperature.

After soaking at this temperature for 10 hrs, the Pt-lid is removed from the crucible and the temperature is reduced to 900^{o}C and is equilibrated at this temperature for about a day. Thorough mixing of the solution is established using a Pt-holder (fork) that is attached to the Alumina rod.

The equilibration to the liquidus temperature is ensured by observing the liquid surface for crystallization and dissolution of crystals and is confirmed by the dipping of non-polished test substrates into the solution. A Pt-basket and an alumina rod are used to remove the crystallites that might have formed on the surface of the melt. The etched substrates that were thoroughly rinsed with distilled water and ethanol are mounted on an alumina rod either vertically or horizontally (Figure 11 and Figure 12) using Pt wires.

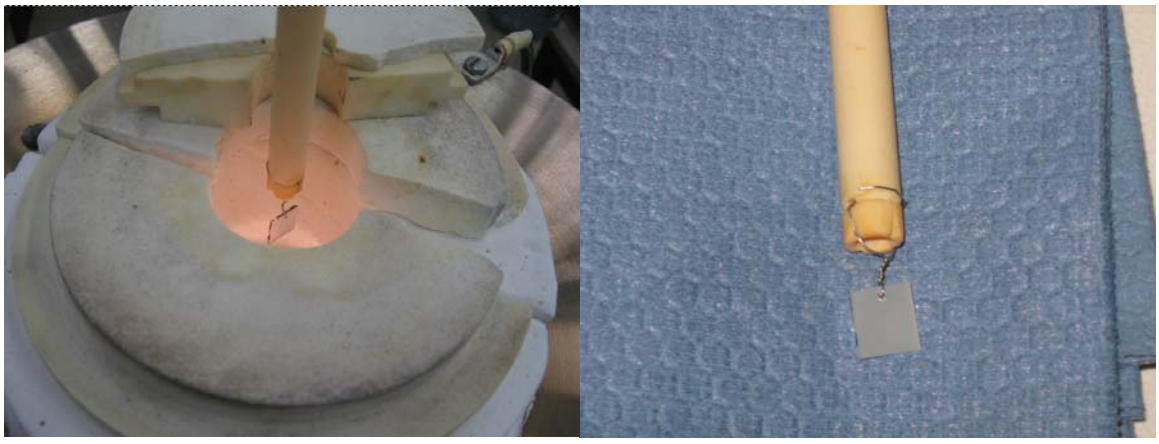

Figure11 Post growth view of vertical substrate settings.

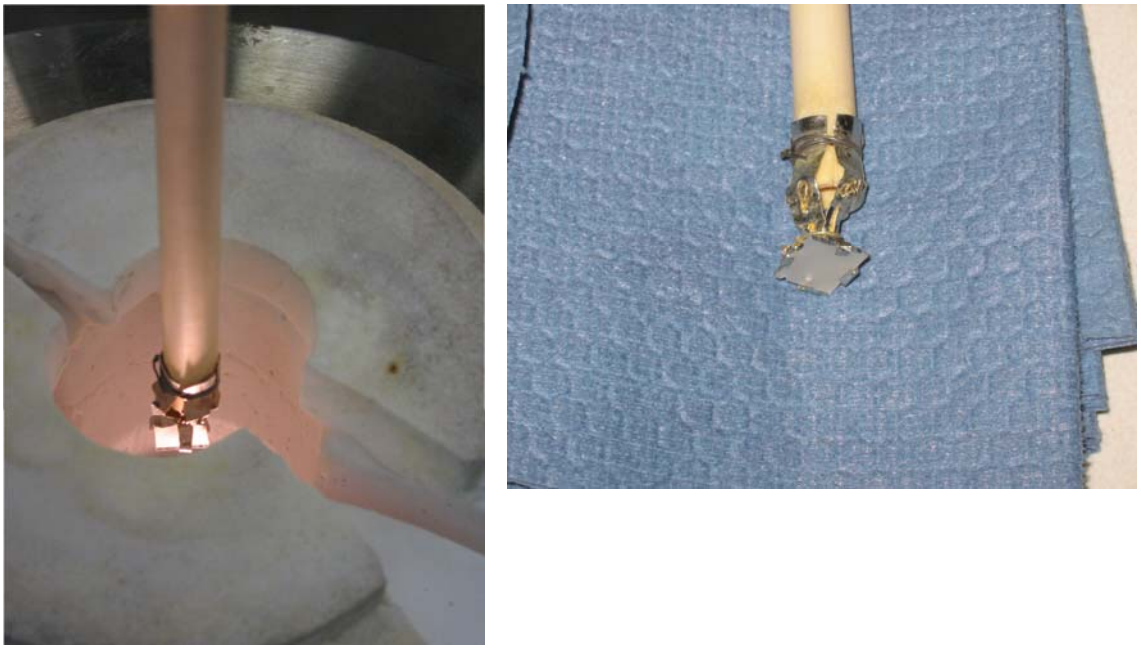

Figure12 Post growth view of horizontal substrate settings.

The substrates are dipped in the solution and rotated at about 80-100 or 15-35 rpm, for horizontally and vertically mounted substrates, respectively. The size and shape of the substrates are the main consideration in deciding the type and speed of the rotation. The growth time is approximately 30 min. In order to remove the flux after the growth, high rotation rates of about 700 rpm are used for horizontally mounted substrates to spin off the liquid, whereas slow substrates withdrawal in order to suppress dynamic wetting effects used for vertically mounted substrates.

CHAPTER 4
FILM CHARACTERIZATION

4.1 Structural characterization

4.1.1 Surface morphology by Nomarski microscopy

Films were grown in three main X-, Y- and Z- orientations. Their surface morphology and growth features were investigated first by the means of optical microscopy. The X-oriented Cr:LGT film grown on X-Cut LGT substrates (Figure 13) showed an extremely smooth surface and presented no cracks.

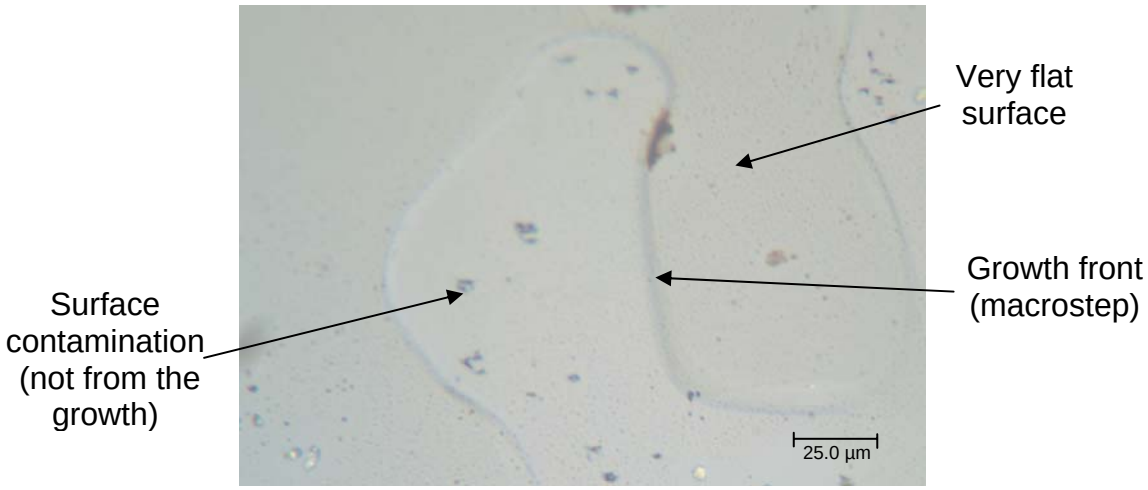

Figure 13 Optical microscopy of X-Cr:LGT film with growth front.

This is an indication of a nearly perfect lattice match between the substrate and the film. The film composition was found almost identical with the substrate composition and no incorporation of solvent ions or other inclusions were noticed. However, some impurities were trapped on the surface and difficult to remove.

As shown in Figure 14, relatively large growth steps were commonly observed on Y-oriented undoped LGT LPE films. The growth steps follow the crystal symmetry with the main steps propagating in <001> and <100> directions. Though there is a tendency to form facets in Y-oriented films due to the existence of other surface orientations, facet development is not clearly evident on these Y-oriented films of the current study.

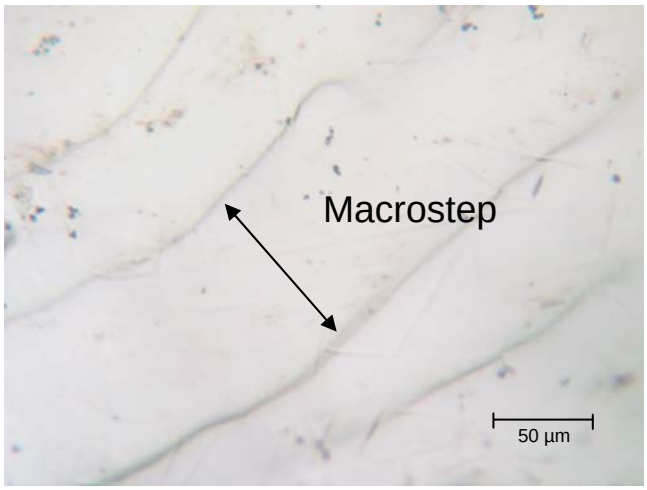

Figure 14 Y-undoped LGT film with macro steps.

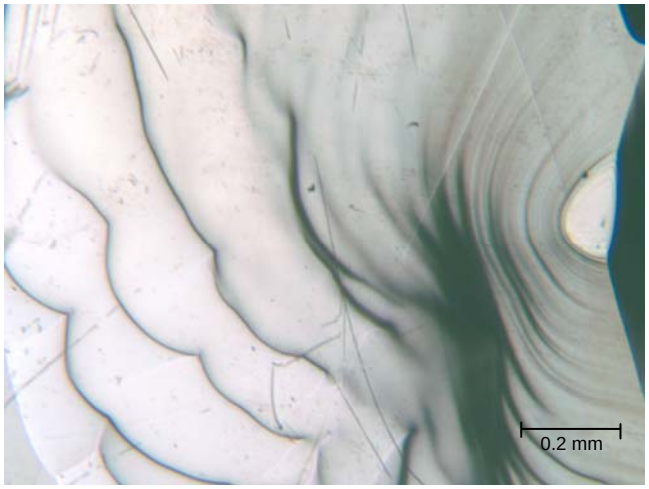

Figure 15 Z-Ti:CrLGT film showing triangular hillock with macro steps.

For the case of Z-oriented Ti:CrLGT films on the substrates of the same orientation, initial growth hillocks formation (Figure 15) that further developed into established growth steps is frequently observed.

This can be clearly explained: The growth morphology in these films show initial triangular and spiral hillocks oriented according to the crystal symmetry. The slopes of these hillocks are mainly due to growth conditions, such as high supersaturation. In the case of lower supersaturation conditions, this may turns into macroscopic spirals development with growth steps extending to atomically flat interstep distances. This is understood from the theory and morphological studies on LPE of other oxides as well.

4.1.2 XRD rocking curve analysis

The crystallinity of the LGT films can be better characterized using the rocking-curve feature of X-ray diffraction (XRD) technique. In this characterization technique, the crystal is rotated through the Bragg angle, and the reflected beam is taken into account by a fixed counter. Crystals with greater perfection exhibit diffraction peak widths which are smaller than those of less perfect crystals.

There appears to be a minimum width of a diffraction peak which depends on the material, the wave length of X–rays, the reflection and other factors. The shape of the diffraction peak i.e. intensity as a function of rotation of the sample crystal, is termed the crystal's rocking curve. The width of the rocking curve presents direct information regarding crystal orientation, because each potentially slightly misoriented subgrain comes into reflection as the crystal rotates. For an

incident plane wave and the reflection setting, dynamical theory predicts a flat-topped rocking curve, known as the Darwin curve, and the width of the flat-top portion of this curve is termed as the Darwin curve width (2s). Peak reflectivities (ratio of diffracted and the incident monochromatic intensities) approaching 100% have been measured for incident plane waves. However it is important to realize that reflectivity drops precipitously if defects are present in the crystal. The FWHM of the Darwin curve represents a limit for a given geometry which can be approached but never exceeded. For a perfect crystal, the theoretical FWHM is around 0.003°.

Very few crystals approach this value naturally. For most single crystals this value is even 10 to 100 times larger than that of this theoretical value. Just as the presence of linear and planar lattice faults decreases reflectivity, these increase the width of the crystal's rocking curve. Measurement of rocking curves is, therefore, an important method for assessing the perfection of crystals and epilayers, particularly those for micro electronic and optical applications.

As mentioned above, rocking curve measurements are considered in this current work to compare relative crystallinity of films and substrates. Figure 16 shows the rocking curve of an X-oriented LGT substrate prepared from a crystal grown by Czochralski Method. A FWHM of 0.0443° was obtained for this sample; indicating a slight disorderness of the crystal.

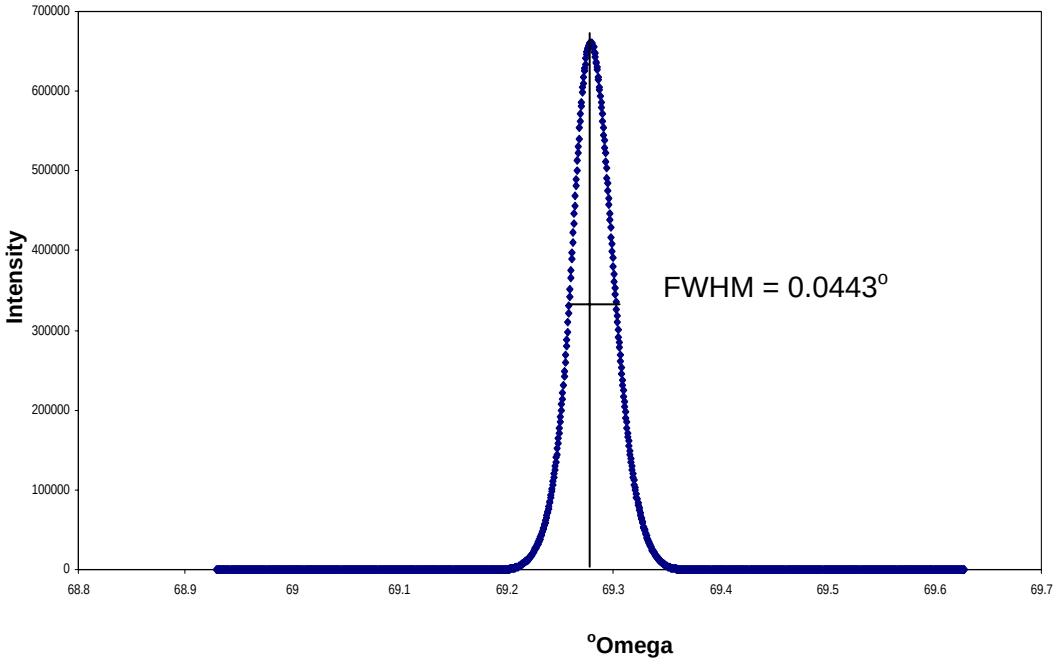

Figure 16 XRD rocking curve for X-LGT substratefor (004) reflection.

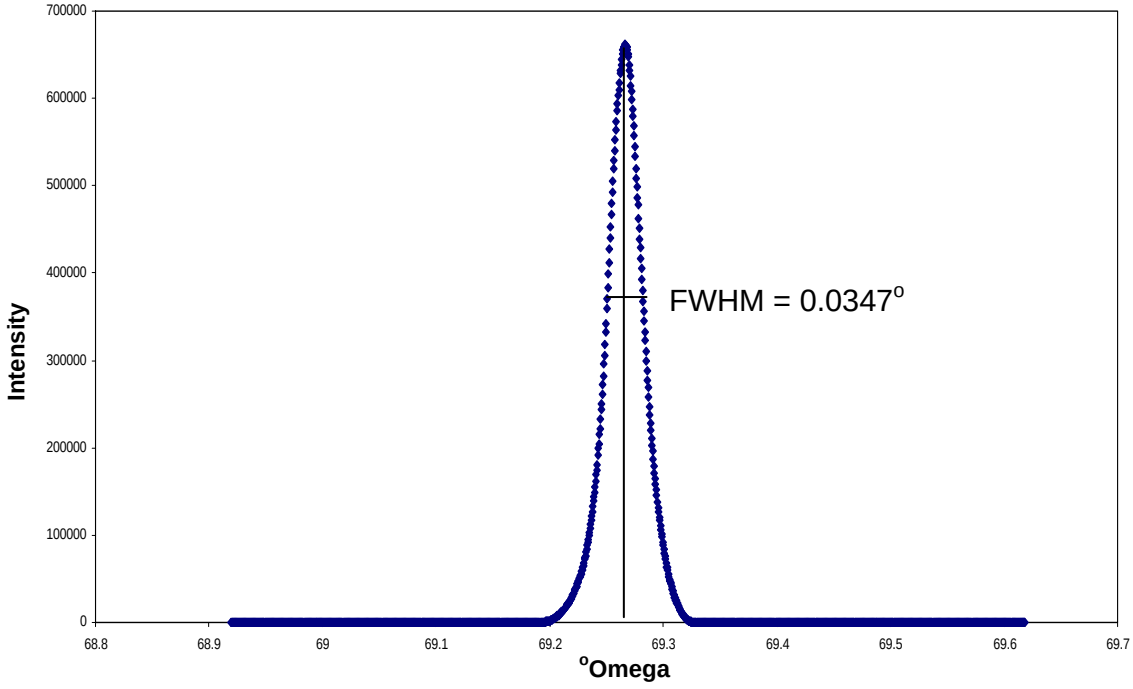

Figure 17 XRD rocking curve of horizontally dipped X-Cr:LGT LPE film of (004) reflection.

Figure 17 shows the rocking curve of a horizontally dipped X-oriented Cr:LGT film. A FWHM of 0.0347° obtained for this film, which indicates better structural perfection than that of the substrate. Figure 18 shows the rocking curve of an Al: Ti: Cr: LGT X-oriented film with a FWHM value of 0.0350°. In fact, the structural perfection of X-oriented LGT films was consistently better than that of LGT substrates used in this study. Also, the surface of these films is very smooth [34].

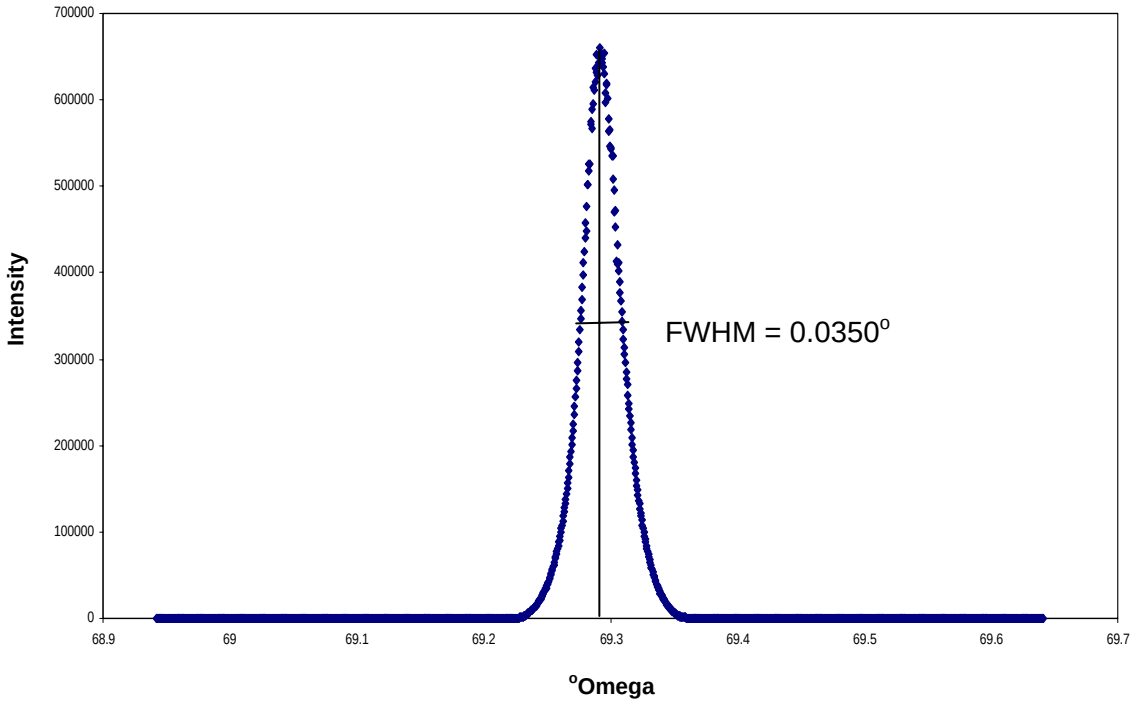

Figure 18 Rocking curve of X-oriented Al:Ti:Cr:LGT LPE film of (004) reflection.

As the Y-oriented films show the tendency of step formation depending on the density of steps and the magnitude of the step bunching the FWHM values are slightly larger and typically around 0.0465°. The rocking curve of a Y-oriented undoped film is shown in the figure 19. These values are quite remarkable for oxide films, and also represent about one order of

magnitude improvement compared to the FWHM of 0.2° obtained for the very first LGS films [29].

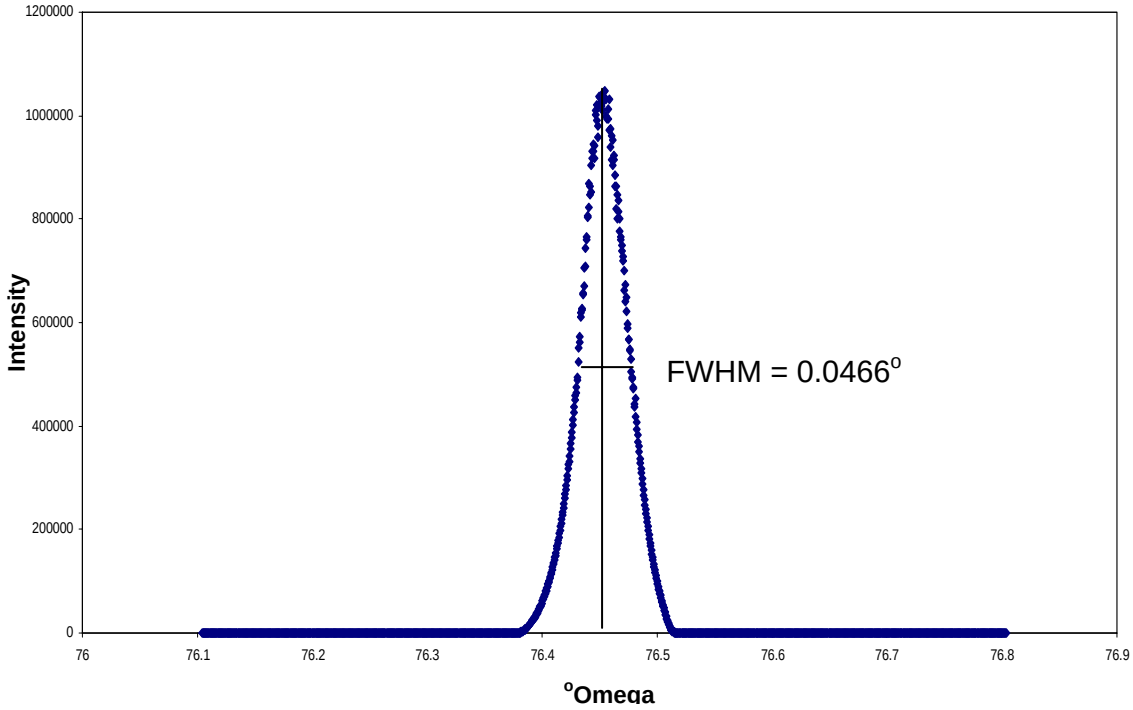

Figure 19 Rocking curve of a Y-undoped LGT film.

4.1.3 TEM studies

Figures 20 to 23 show the transmission electron microscopy (TEM) images of the Ti, Cr doped LGT film during the current study.

Figure 20 represents a cross section of the TEM-sample that was prepared using the focused ion beam (FIB) technique. The layer sequence of this sample are: Pt-layer for FIB lift out, Au-Pd sputter coating layer for the purpose of continuous electrical conductive sample during FIB sample preparation, thick LGT film and LGT substrate.

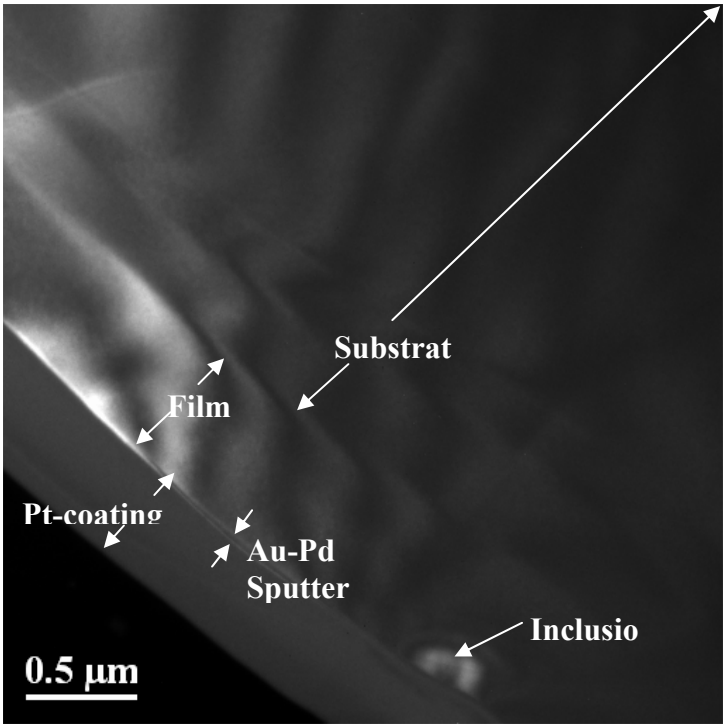

Figure 20 TEM image of X-Ti:Cr LGT film and substrate

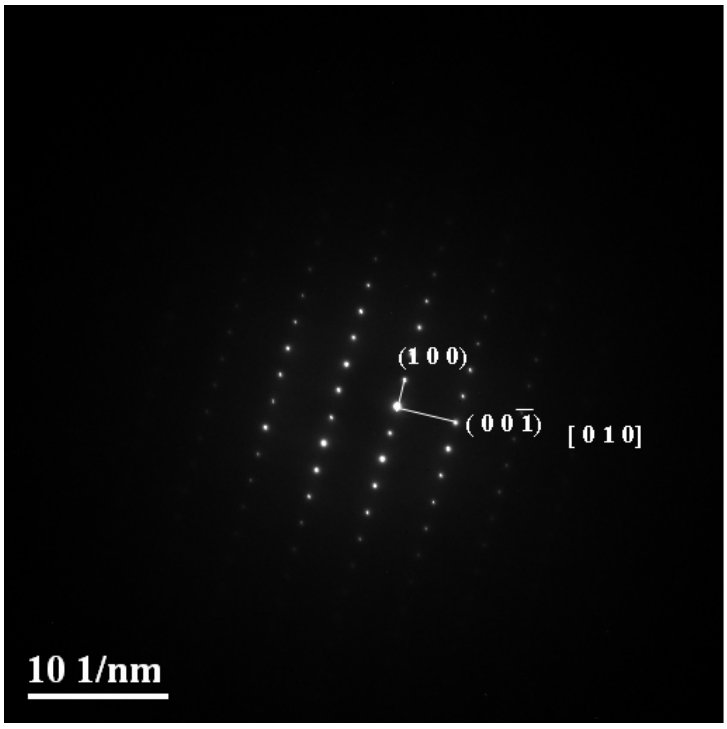

Figure 21 Diffraction pattern of X- Ti:Cr LGT film.

The continuous lattice of the film during homoepitaxial film growth with the substrate is evident from the continuous bending contour lines on both film and substrate layers. Figure 21 shows the selected area diffraction (SAD) pattern of the film cross section that is characteristic of the single phase, single crystalline and defect free material. The [010] zone axis is the indication of the X-oriented film growth on the substrate crystal. No defects and second phase particles are observed from this diffraction pattern. Figure 23 shows higher-order Laue zone (HOLZ) lines formed by elastic scattering of a convergent electron beam in the central 000 diffraction disc of the LGT film and figure 24 for that of the LGT substrate material.

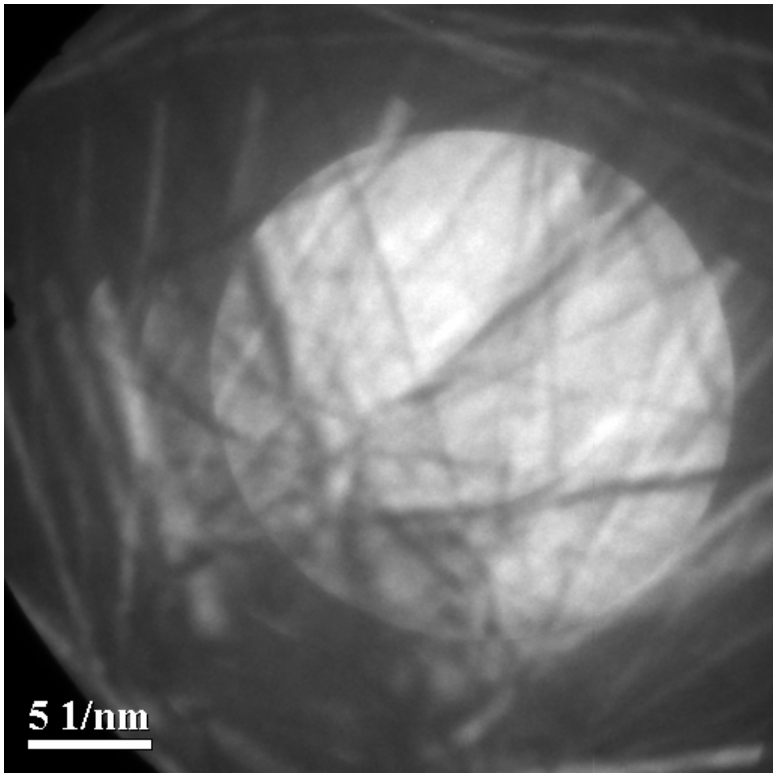

Figure 22 HOLZ Lines taken on the LPE film

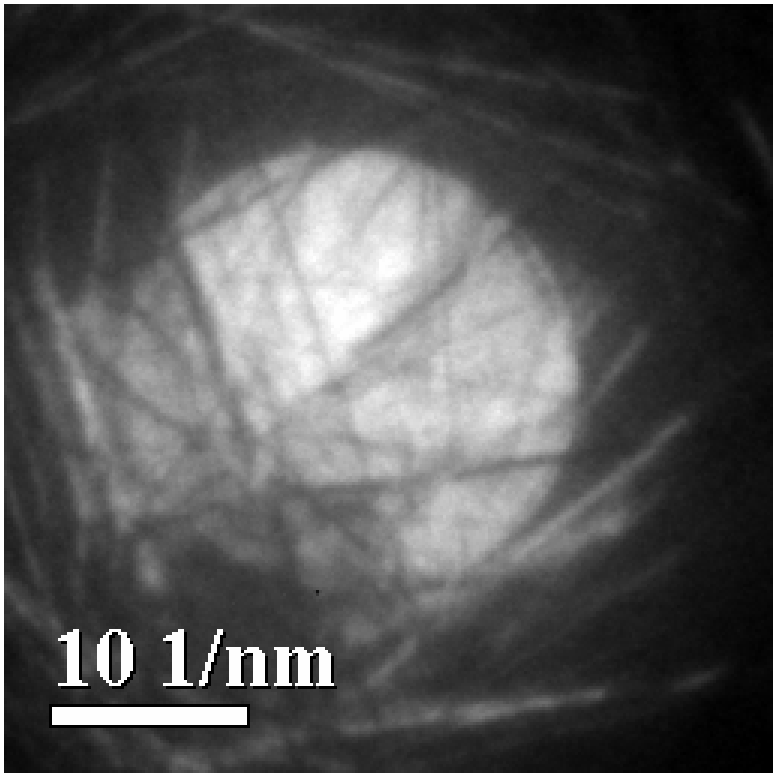

Figure 23 HOLZ lines of taken on the substrate.

From the above figures, it is known that the film has same crystal orientation as substrate and the lattice parameter difference is less than 0.01%. From HOLZ lines it is clear that the region is defect free.

In general, it is possible to assess the accurate zone axis of the film by extending these HOLZ lines to form an established HOLZ-pattern.

4.2 Chemical characterization

For the bulk compositional analysis and depth profiles of trace elements, dynamic SIMS is used.

4.2.1 Quantitative SIMS results

In order for quantitative measurement of Cr and Ti dopant concentrations in the films comparison in means of standards is required. Dopants are added to the growth solution and incorporated during growth i.e., in-situ growth of doped films.

A process of introducing impurities into the near-surface regions of solids by directing a beam of ions at the solid is known as ion implantation. In this present work, Cr and Ti ions implanted, using ion-implantation technique, in the LGT substrates served as standards for this purpose.

Figure 24 below is the SIMS profile for Cr and Ti dopants implanted X oriented substrates of LGT.

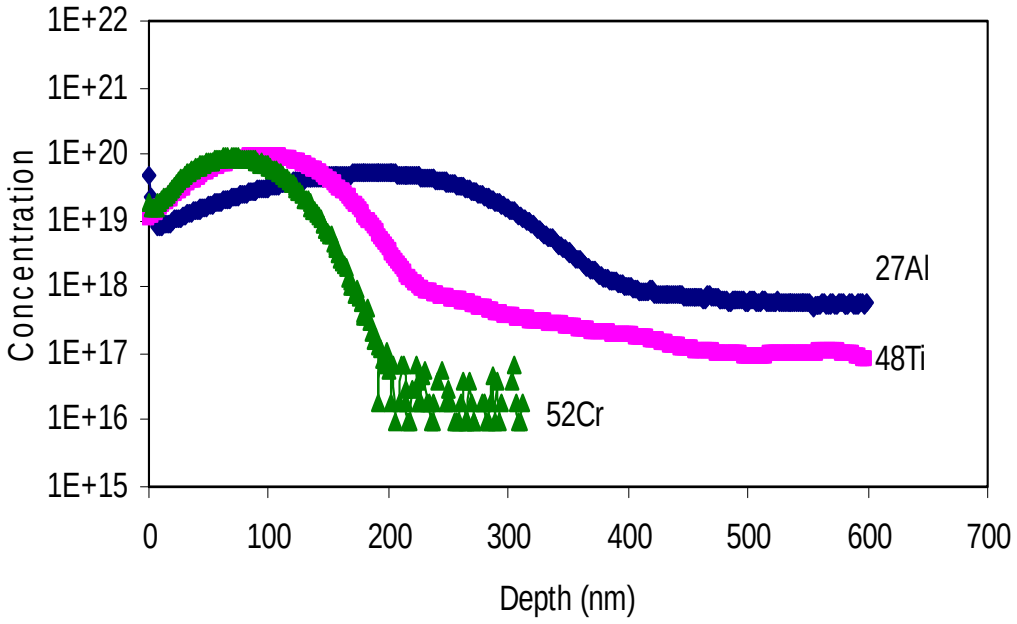

Figure 24 SIMS profile of Ti:Cr co-implanted X LGT substrate

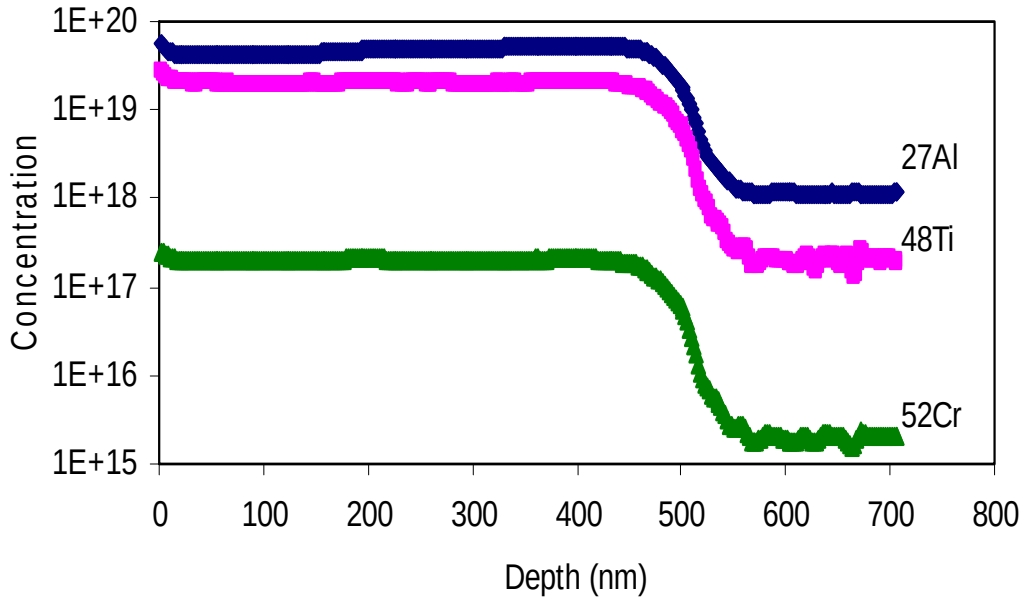

Figure 25 SIMS profile of Ti:Cr doped LGT LPE film

Figure 25 shows the SIMS profiles of Ti and Cr dopants in X-oriented LGT-LPE film.

From Figure 25, it is noticed that Ti is uniformly distributed through out the film thickness with an almost constant concentration.

But it is not the case with Cr concentration and from the profile it is evident that, the amount of Cr that is diffused into the film is very less. Perhaps, the reasons might be slow diffusing characteristics of Cr in addition to the lower driving force as a concentration gradient available for its diffusion.

In both Ti and Cr profiles, there is a sudden decrease in the concentration at the film-substrate interface. The thickness of the film is about 515nm. The mean dopant concentrations of ^{27}Al in the depth range of 250-400 nm is $5.03x10^{19}$atoms/cc, ^{48}Ti is $2.08x10^{19}$atoms/cc and for ^{52}Cr the average value is $3.327x10^{17}$atoms/cc. The corrected values for Ti and Cr, if the isotopic abundance is taken into account, are $3.69x10^{19}$atoms/cc and $3.97x10^{17}$atoms/cc, respectively. The thickness of the film can be varied by varying the growth parameters like growth temperature, growth time, supersaturation and substrate rotation velocity.

Figure 26 is the SIMS profile for horizontally grown X-oriented LGT film. In this the dopant element is only Cr. The average concentration of the dopant is $1.22x10^{17}$atoms/cc. The thickness of the substrate is more when compared to the first film (Figure 25) and is approximately 1.3μm. If the isotopic abundance has to be preserved, the exact value of the Cr concentration is $1.5x10^{17}$atoms/cc.

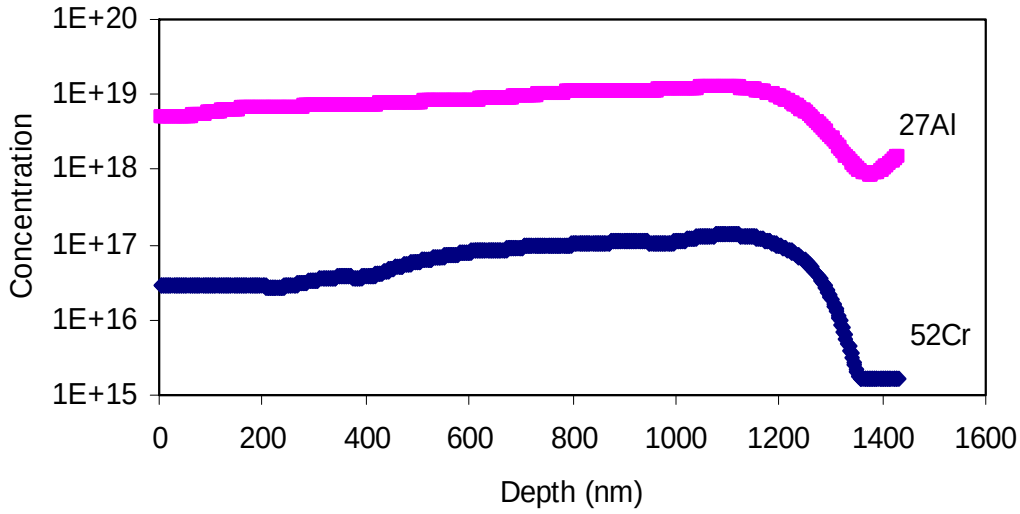

Figure 26 SIMS profile of X-oriented LGT film.

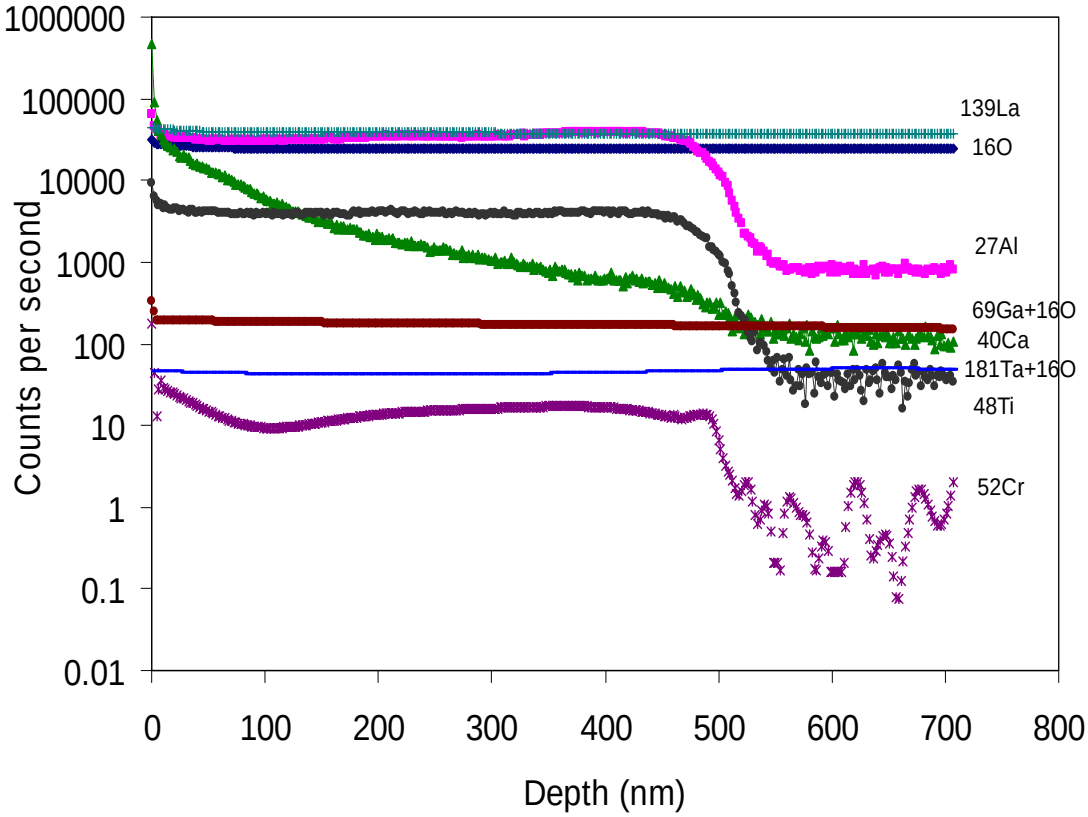

Figure 27 SIMS profile of X-oriented LGT film

From Figure 27, it should be noted that Al and Ca are the two impurities incorporated in the film. Al is distributed uniformly similar to Ti. In contrast, the Ca concentration is high at the surface and decreases gradually. This might indicate a segregation coefficient different from unity. Cr is added as a dopant element, it is incorporated into the film in a little quantity.

PbO could not be detected by the characterization techniques used. Therefore, it is assumed that PbO is not incorporated into the LGT film lattice. Even in the main constituents, there is a slight change in the composition from film to the substrate. It is observed that the Ta concentration in the substrate is slightly higher than that found in the film.

4.3 Optical characterization

The as-grown film of Y-orientation is used for the transmittance investigation. For this Varian Cary 500 Spectrophotometer was used. The transmittance spectrum was measured from the wavelength 200-3300 nm and the absorption edge was determined. The transmittance spectrum of LPE LGT film with Y-orientation is shown in figure 28. The transmittance of the film is found to be approximately 80% which is comparable with the transmittance value of the LGT Czochralski grown polished crystal [42].the highest transmittance is observed in the range of 600 to 2700 nm wavelength. The absorption edge value is 247nm.

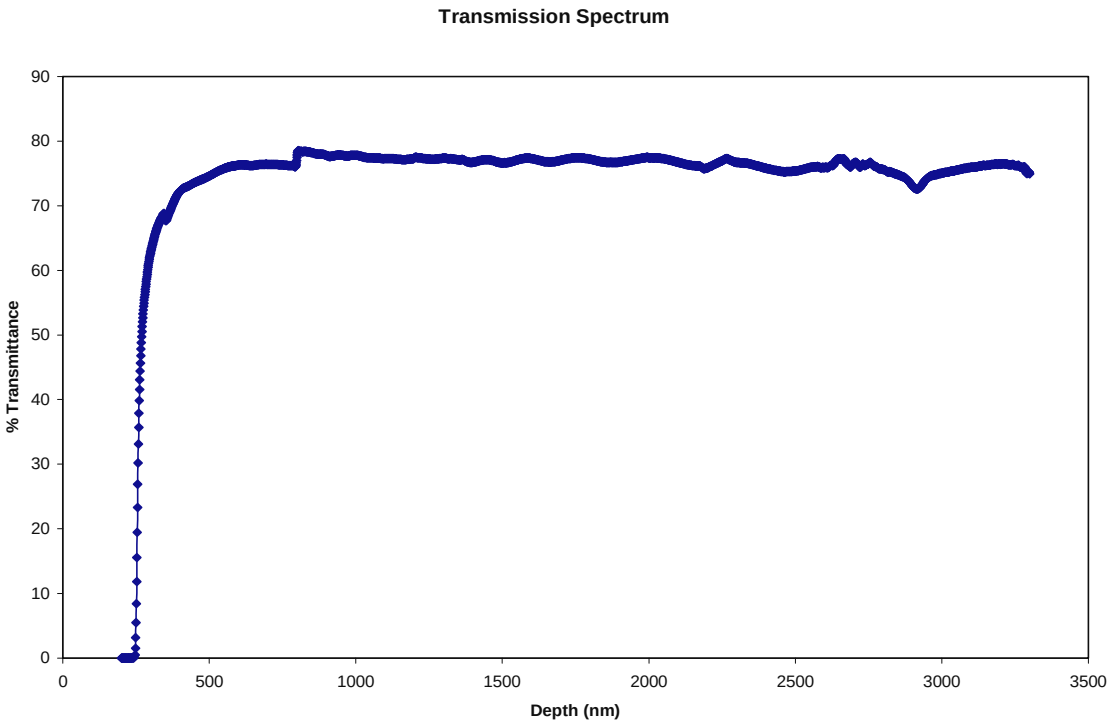

Figure 28 Transmission spectrum for Y-oriented film

CHAPTER 5
DISCUSSIONS

Factors related to site occupancy of dopant atoms- Al, Ti, Cr and Ca in comparison with the constituent elements (highlighted): La, Ga, Ta and O of the LGT crystal are reported in Table 3. The close matching of co-ordination number, electron valence, ionic radius and electronegativity details between any two elements (actual element vs. dopant) can be inferred as the dopant's tendency to occupy that particular site.

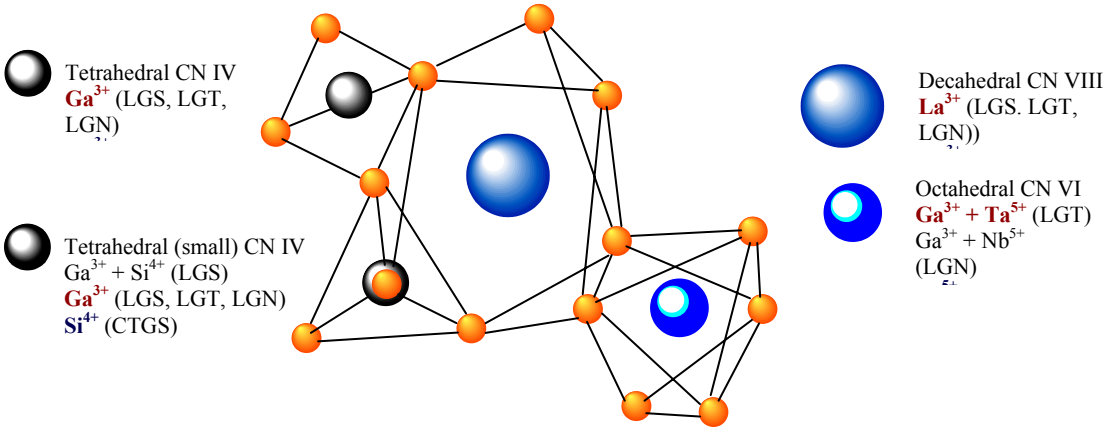

Figure 29 LGT structure with different atomic positions.

As shown in figure 29, the La^{3+} atoms are situated in the decahedral sites surrounded by 8 oxygen atoms. Ga1 occupy the octahedral site with six oxygen atoms surrounding it. Ga2 and Ga3 occupy the tetrahedral sites with the coordination number IV for each of them.

Ca for its both coordination numbers (VI and VIII) has comparable atomic sizes and electro-negativity values existed with the La atoms. Also, the difference in their respective electron valances for Ca vs. La atoms is negligible. For these reasons, Ca is expected to occupy La sites.

But, Ca is clearly departing in either of the factors for rest of the elements in showing any possibility to occupy their sites. So, La sites are the only greatest possibility for Ca atoms.

Cr on the other hand has 3 different coordination number possibilities (IV, VI and VIII), of which Cr with VI-coordination number and +2-electron valence has some direct tendency to occupy Ga1 sites. Deviation in electron valence by 1 electron and electronegativity by 1.5eV are the restrictions for this position occupation.

Table 3 Substitutional solubility assessments of various elements.

Element	Co-ordination Number	Electron Valence	Ionic Radius (Å)	Electro-negativity (eV)
La	VIII	+3	**1.160**	1.1
Ga	IV	+3	**0.47**	1.6
	VI	+3	**0.620**	
Ta	VI	+3	0.72	1.5
		+4	0.68	
		+5	**0.64**	
Al	IV	+3	0.39	3
	VI	+3	**0.535**	
Ti	IV	+4	0.42	4
	VI	+2	0.86	
		+3	**0.67**	
		+4	**0.605**	
Cr	IV	+4	0.41	3
		+5	0.345	
		+6	0.26	
	VI	+2	0.73	
		+3	**0.615**	
		+4	**0.55**	
		+5	0.49	
		+6	0.44	
Ca	VIII	+2	1.12	2

But, due to their small ionic radii size, Cr with its IV coordination number has possibility to occupy Ga3 sites, provided the deviations in electron valence by 1 or more than 1 electron and electronegativity by 1.5eV are not the great constraints.

Similarly, Cr with VI-coordination number and ionic radius of 0.615 Å may show slight tendency to occupy Ga1 sites solely because of electron valence and ionic radius size matching.

Ti with its IV-coordination number and ionic radius of 0.42 Å may only negligible possibility to occupy Ga3 sites. But, VI-coordintation number value and +3 electron valence combinations of Ti shows good tendency to occupy Ga1 sites. If ionic radii are the only consideration, all Ti atoms with above 0.65 Å size occupy Ga1 sites and within 0.6 to 0.65 Å size range occupy Ga2 sites.

Both Al-atoms with different coordination number have few chances to occupy Ga3 sites due to their good matching in electron valence. However, Al with IV coordination number is comparatively better in this aspect. With respect to the ionic radius, the smaller the radius the better the tendency to incorporate into the film. Al is the smallest species among the other dopant elements. This may be the reason for the higher concentration of Al dopant in the films.

It is not possible to grow LGT crystals from the PbO flux used for LPE technique during seedless growth process of the films. It is postulated that the growth does not proceed in the primary crystallization field (PCF) of LGT [25**,** 34]. Thus, these LGT crystals start growing in a two phase region where both LGO and LGT phases, can coexist, rather than the single phase

LGT region of the phase diagram. Consequently, when LGT substrate provides seed for nucleation, the magnitude of the strain energy is too large to allow epitaxy of LGO, this causes langasite phase to crystallize preferentially.

Supersaturation control process becomes challenging, when LGO crystals form during temperature controlled melting in the higher temperature range. Because, these LGO crystals hinder the growth process of LGT films using LPE technique. LGO formation could be reduced to very good extent by the close control of the flux temperature processing. In case of insufficient initial supersaturation, etch-back and regrowth are the consequences observed with the earlier experiments. This is due to the fact, that substrate dissolution is favored with respect to film growth, especially for metastable growth conditions.

CHAPTER 6
SUMMARY AND CONCLUSIONS

From the parameters given in table 1, the effective growth rate of the film is calculated as 1.387 Å/s, and the maximum stable growth rate, calculated using equations 1.14 & 1.15, with values from Table 1, is found to be 349 Å/s which is 200 times more than that of the linear growth rate. Since the experimental growth rate is lower than the maximum stable growth rate, we can postulate that the films have no inclusions. This was further confirmed by the TEM studies. We observed some surface contamination, and residual solvent, though.

The crystallinity of the film material is very high, as found from the FWHM value of the XRD rocking curve (0.0347^{o}), which is also is supported by the TEM studies.

The initial volume of the substrate can be estimated to be about 0.1 cc, and the quantity of the material is 0.615g. The quantity of the material deposited as film on the LGT substrate is calculated as 0.31 mg. Hence, the volume of the film is about $5x10^{-5}$ cc. For LGT, the total number of atoms per cc is $7.52x10^{22}$. The percentage of dopants Al, Ti and Cr added to the solution (i.e., initial concentration of all dopants) is 0.4%. The typical dopant concentration found in a film is 0.09% of which Al represents 0.066%, Ti 0.027% and Cr 0.001%. These are approximate values, valid for the experimental conditions applied in this study.

The optical transmittance of the film is approximately 80% which is good and comparable with the value of LGT polished substrate.

This study did focus on the growth and structural and chemical characterization of LPE grown LGT films doped with different ions. We have demonstrated that a very homogeneous dopant concentration can be achieved, while preserving the excellent crystallinity and homogeneity of the material.

Herein, we have investigated co-doping with 4 ions: Al, Ti, Cr, and Ca. Whereas co-doping with Al and Ti had been investigated in a previous study, we have extended the research to include Cr and Ca. Co-doping by more than one ion can significantly affect the growth morphology of the films. We have successfully demonstrated that a very homogeneous doping by Cr ions in LGT is possible. In future study, the oxidation state of Cr could be investigated, as Cr^{4+} doped LGT could lead to the development of eye-safe lasers (LGT is also a laser host material). We also found that the Ca concentration in the film was not homogeneous, which could indicate a segregation coefficient different from unity for this dopant.

Since high-quality films are now available, future studies on piezoelectric properties of the films become possible. In addition, doping studies could be extended to other ions. The knowledge of the impact of various dopants on the properties of the LGT material could allow the design of material with superior properties, for example to fulfill specific device requirement.

REFERENCES

1. H. Nelson, “Epitaxial growth from the liquid state and its application to the fabrication of tunnel and laser diodes”, RCA Review, 24, 603 (1963).
2. S.L. Blank and J.W. Nielsen, “The growth of magnetic garnets by liquid phase epitaxy”, J. Cryst. Growth 17, 302 (1972).
3. P.K. Tien, R.J. Martin, S.L. Blank, S.H. Wemple, L.J. Varnerin, “Optical waveguides in single-crystal garnet films”, Appl. Phys. Lett. 21, 207 (1972).
4. B. Ferrand, B. Chambaz, and M. Couchaud, “Liquid phase epitaxy: A versatile technique for the development of miniature optical components in single crystal dielectric media”, Opt. Mater. 11, 101 (1999).
5. L.I. Ivleva, D.T. Kiselev, Y.S. Kuzminov, N.M. Polozkov, "Growth and study of barium metaborate single crystals", Inorg. Mater. 24, 982 (1988).
6. W.K. Burton, N. Cabrera, and F.C. Frank, “The growth of crystal and the equilibrium structure of their surfaces”, Phil. Trans. A 243, 299 (1951).
7. N. Cabrera and M.M. Levine, “On the dislocation theory of evaporation of crystals”, Phil. Mag. 1, 450 (1956).
8. E. Bauser, in: Handbook of crystal growth, edited by D.T.J. Hurle, Vol3a, Elsevier, Amsterdam, 1994.
9. C. Klemenz and H.J. Scheel, “Crystal growth and epitaxy from solutions”, Mater. Sci. Forum 276-277, 175 (1998).
10. E. Bauer, Z. Kristallogr. 110, 395 (1958).

11. F.C. Frank and J.H. Van der Merwe, “One-dimensional dislocations. 1. Static theory”, Proc. R. Soc. London A 198, 205, (1949).
12. M. Volmer and A. Weber, Z. Phys. Chem. 119, 277 (1926).
13. J.N. Stranski and L. Krastanov, Ber. Akad. Wiss. Wien 146, 797 (1938).
14. A.A. Chernov, “Notes on interface kinetics 50 years after Burton, Cabrera and Frank”, J. Cryst. Growth 264, 499 (2004).
15. E.L. Belokoneva, M.A. Simonov, A.V. Butashin, B.V. Mill, N.V. Belov, “Crystal Structure of Calcium gallogermanate $Ca_3Ga_2Ge_4O_{14}$=Ca_3Ge [(Ga_2Ge) Ge_2O_{14}] and its analog $Ba_3Fe_2Ge_4O_{14}$=Ba_3Fe [$(FeGe_2)$ Ge_2O_{14}]”, Sov. Phys. Dokl 27, 954 (1980).
16. Mitch M.C. Chou, “Piezoelectric crystals, $La_3Ga_{5.5}Ta_{0.5}O_{14}$ (LGT), $La_3Ga_{5.5}Nb_{0.5}O_{14}$ (LGN), $La_3Ga_5SiO_{14}$ (LGS)”, Ph.D. Thesis, University of Central Florida (2000).
17. A.A. Kaminskii, B.V. Mill, G.G. Khodzhabagyan, A.F. Konstaninova, A.I. Okorochkov, I.M. Silvestrova, “Investigation of trigonal $(La_{1-x}Nd_x)_3SiO_{14}$ crystals: I growth and optical properties”, Phys. Stat. Sol (a) 80, 387 (1983).
18. A.A. Kaminskii, “On the laws of crystal-field disorder of Ln^{3+} ions insulating crystals”, Phys. Stat. Sol (a) 102, 389 (1987).
19. Mark H. Randles, John E. Creamer, “Disordered oxide crystal hosts for diode pumped lasers”, J. Cryst. Growth 128, 1016 (1993).
20. H. Takeda, K. Sugiyama, K.Inaba, K. Shimamura, T. Fukuda, “ Crystal growth and structural characterization of new piezoeletric material $La_3Ga_{5.5}Ta_{0.5}O_{14}$”, Jpn. J. Appl. Phys. 36, L919 (1997).

21. J.J. Hsieh, “Thickness and surface morphology of GaAs LPE layers grown by supercooling, step-cooling, equilibrium cooling, and two-phase solution techniques”, J. Cryst. Growth 27, 49 (1974).
22. J.M. Robertson, “Liquid phase epitaxy of garnets”, J. Cryst. Growth 45, 233 (1978).
23. R. Ghez, E.A. Giess, “Liquid phase epiataxial growth of magnetic garnet films grown by isothermal dipping with axial rotation”, Mat. Res. Bull. 8, 31 (1973).
24. D. Elwell, H.J. Scheel, “Crystal growth from high temperature solutions”, Academic press, London (1975).
25. C.F. Klemenz and D.C. Malocha, “Epitaxial Films of LGS, LGT and LGN for SAW and BAW devices”, IEEE Intl. Fre. Ctrl. Symposium, 301 (2003).
26. C. Klemenz, “High quality langasite films grown by liquid phase epitaxy”, J. Cryst. Growth 237-239, 714 (2002).
27. Bruce H. T. Chai, Mitch M. C. Chou, Haihong Qiu and Shen Jen, “Electronic device including langasite structure compounds and method for making same; crystal photonics”, www. patentstorm.us/ assignees /crystal_ photonics, _ incorporated-86737-1.html.
28. S.B. Austerman, J. Nucl. Mater. 14, 225 (1964).
29. C. Klemenz, “Liquid phase epitaxy of $La_3Ga_5SiO_{14}$”, Proc. 15th Euro. Frequency & Time Forum, 714 (2001).
30. R.D. Shannon, Acta Crystallogr. A32, 751 (1976).
31. M.H. Randles, C.J.M. Roojimans (Ed.), “Crystals: growth, properties and applications, crystals for magnetic applications”, Springer New York 1, 71 (1978).

32. S.L. Blank, “Crytsal growth:magnetic garnets by liquid phase epitaxy”, JEMMSE, The Pennsylvania State University (1979).
33. B.E. Watts, H. Dabkowska, B.M. Wanklyn, J. Cryst. Growth 94, 125 (1989).
34. C. Klemenz, “High-quality $La_3Ga_{5.5}Ta_{0.5}O_{14}$ and $La_3Ga_{5.5}Nb_{0.5}O_{14}$ LPE films for oscillators and resonators”, J. Cryst. Growth 250, Issues 1-2, 34-40 (2003).
35. L.G. Schulz, Acta Crystallogr. 4, 487 (1951).
36. C.F. Klemenz, A. Sayir, In-situ Al:Ti-co-doped $La3Ga5.5Ta0.5O14$ Films for High-Q Resonators, IEEE Intl. Frequency Control Symposium, Miami FL, USA, 676 (2006).
37. R. Sum, H.P. Lang, H.-J. Guntherodt, “Scanning force microscopy study of single-crystal substrates used for thin-film growth of high-temperature superconductors”, Physica C: Supercond 242 Issues 1-2, 174 (1995).
38. S. Laffey, M. Hendrickson and J.R. Vig, “Polishing and etching langasite and quartz crystals, IEEE Fre. Ctrl. Symp, 245 (1994).
39. A.N. Gotalskaja, Dresin, S.N. Schegolkova, N. Saveleva, V. Bezdelkin, G. Cherpoukhina, **“**Langasite crystal quality improvement aimed at high-Q resonator fabrication”, IEEE Fre. Ctrl. Symp, 657 (1995).
40. C.Klemenz, “Liquid phase epitaxy of YBCO and NdBCO High Tc- superconductors”, Ph. D Thesis Nr. 14645, The University of Tokyo (2000).
41. Hans J. Scheel, Tsuguo Fukuda, “Crystal growth technology”, John wiley and sons, 626 (2003).

42. Haikuan Kong, Jiyang Wang, Huaijin Zhang, Xin Yin, Xiufeng Cheng, Yanting Lin, Xiaobo Hu, Xiangang Xu, Minhua Jiang, "Growth and characterization of $La_3Ga_{5.5}Ta_{0.5}O_{14}$ crystal", Cryst. Res. Tech. 39, 686 (2004).
43. Yaroslav Romanyuk, "liquid-phase epitaxy of doped $KY(WO_4)_2$ layers for waveguide lasers", Ph.D. thesis, No 3390, Ecole Polytechnique Federale de Lausanne (2005).
44. Bindu M. Sreeramakavacham, Christine F. Klemenz, "Liquid phase epitaxial growth of Langatate thin films", Proceedings of the Intl. Symp. for scholars on metallurgy, materials science and engineering, Chennai, India, 678 (2006).